Integration of velocity-dependent spatio-temporal structure of place cell activation during navigation in a reservoir model of prefrontal cortex

Pablo Scleidorovich, Alfredo Weitzenfeld, Jean-Marc Fellous, Peter Ford Dominey

Biological Cybernetics
https://doi.org/10.1007/s00422-022-00945-6

Biological Cybernetics

ORIGINAL ARTICLE

Integration of velocity-dependent spatio-temporal structure of place cell activation during navigation in a reservoir model of prefrontal cortex

Pablo Scleidorovich[3] · Alfredo Weitzenfeld[3] · Jean-Marc Fellous[4] · Peter Ford Dominey[1,2]

Received: 7 February 2022 / Accepted: 10 September 2022

Abstract
Sequential behavior unfolds both in space and in time. The same spatial trajectory can be realized in different manners in the same overall time by changing instantaneous speeds. The current research investigates how speed profiles might be given behavioral significance and how cortical networks might encode this information. We first demonstrate that rats can associate different speed patterns on the same trajectory with distinct behavioral choices. In this novel experimental paradigm, rats follow a small baited robot in a large megaspace environment where the rat's speed is precisely controlled by the robot's speed. Based on this proof of concept and research showing that recurrent reservoir networks are ideal for representing spatio-temporal structures, we then test reservoir networks in simulated navigation contexts and demonstrate they can discriminate between traversals of the same path with identical durations but different speed profiles. We then test the networks in an embodied robotic setup, where we use place cell representations from physically navigating robots as input and again successfully discriminate between traversals. To demonstrate that this capability is inherent to recurrent networks, we compared the model against simple linear integrators. Interestingly, although the linear integrators could also perform the speed profile discrimination, a clear difference emerged when examining information coding in both models. Reservoir neurons displayed a form of statistical mixed selectivity as a complex interaction between spatial location and speed that was not as abundant in the linear integrators. This mixed selectivity is characteristic of cortex and reservoirs and allows us to generate specific predictions about the neural activity that will be recorded in rat cortex in future experiments.

Keywords Reservoir computing · Prefrontal cortex · Rat · Navigation · Robotics · Mixed selectivity

1 Introduction

Time is at the heart of all living activities (Lashley 1951). Extensive research has addressed the neurophysiology and modeling of time (see reviews in (Mauk & Buonomano 2004; Paton & Buonomano 2018)), including the ability of recurrent networks to generate population activities that can be associated with elapsed time (Buonomano & Laje 2010; Dominey 1998b; Laje & Buonomano 2013). By their nature, recurrent networks mix their inputs to generate high-dimensional distributed representations. The neural correlate of these high-dimensional representations has been observed in the primate cortex, and it is characterized by mixed selectivity, where cells can concurrently encode multiple task-relevant properties, such as space and task context (Enel et al 2016; Rigotti et al 2013). Recurrent networks have likewise been shown to encode temporal integration properties in sensorimotor sequence learning and time discrimination (Dominey 1998a, b).

In this work, we model spatio-temporal integration based on rat studies involving the dynamic co-navigation between a rat and a robot by manipulating the speed and trajectory of spatial navigation in an open "megaspace" (Gianelli 2018;

Communicated by Benjamin Lindner.

✉ Peter Ford Dominey
peter.dominey@inserm.fr

1 INSERM UMR1093-CAPS, Université Bourgogne Franche-Comté, UFR Des Sciences du Sport, 21000 Dijon, France

2 Robot Cognition Laboratory, Institute Marey, Dijon, France

3 Department of Computer Science and Engineering, University of South Florida, Tampa, USA

4 Departments of Psychology and Biomedical Engineering, University of Arizona, Tucson, USA

Published online: 12 October 2022

Harland et al 2021). Using these techniques, we add a new controllable temporal dimension to behavior that we manipulate in order to study coding principles in the prefrontal cortex (PFC). We use a spatio-temporal reservoir model of the PFC (described below) to assess whether the neural coding can differentiate between conditions where identical paths (i.e., same spatial structure) are navigated with different speed profiles (i.e., different temporal structures). The overview of the system is illustrated in Fig. 1.

Our hypothesis is that the PFC displays coding characteristics that can be simulated by recurrent neural networks of the reservoir type (Lukosevicius & Jaeger 2009). We believe that reservoirs are particularly well suited to simulating the PFC because both reservoir models and primate frontal cortex have been shown to display high-dimensional mixtures of spatio-temporal task-relevant parameters (Rigotti et al 2013). Our long-term goal is to determine whether the rat PFC behaves computationally as a recurrent network in its ability to integrate serial temporal structure during spatial navigation in which travel speed is controlled. Thus, in the current research, we test the hypothesis that a recurrent network will generate mixed spatial and temporal selectivity during exposure to different spatio-temporal navigation sequences in a megaspace environment.

To assess our hypothesis, we first perform an experiment demonstrating that rats can indeed use speed information on identical paths to make navigation decisions. This experiment is a demonstration of the possibility that rats are sensitive to velocity, which motivates us to ask how speed might be represented in a recurrent model of PFC. We then develop and test the speed-integration capabilities of computational models integrating hippocampus (HIPP)-PFC activity. To better assess the model under more realistic conditions, we perform

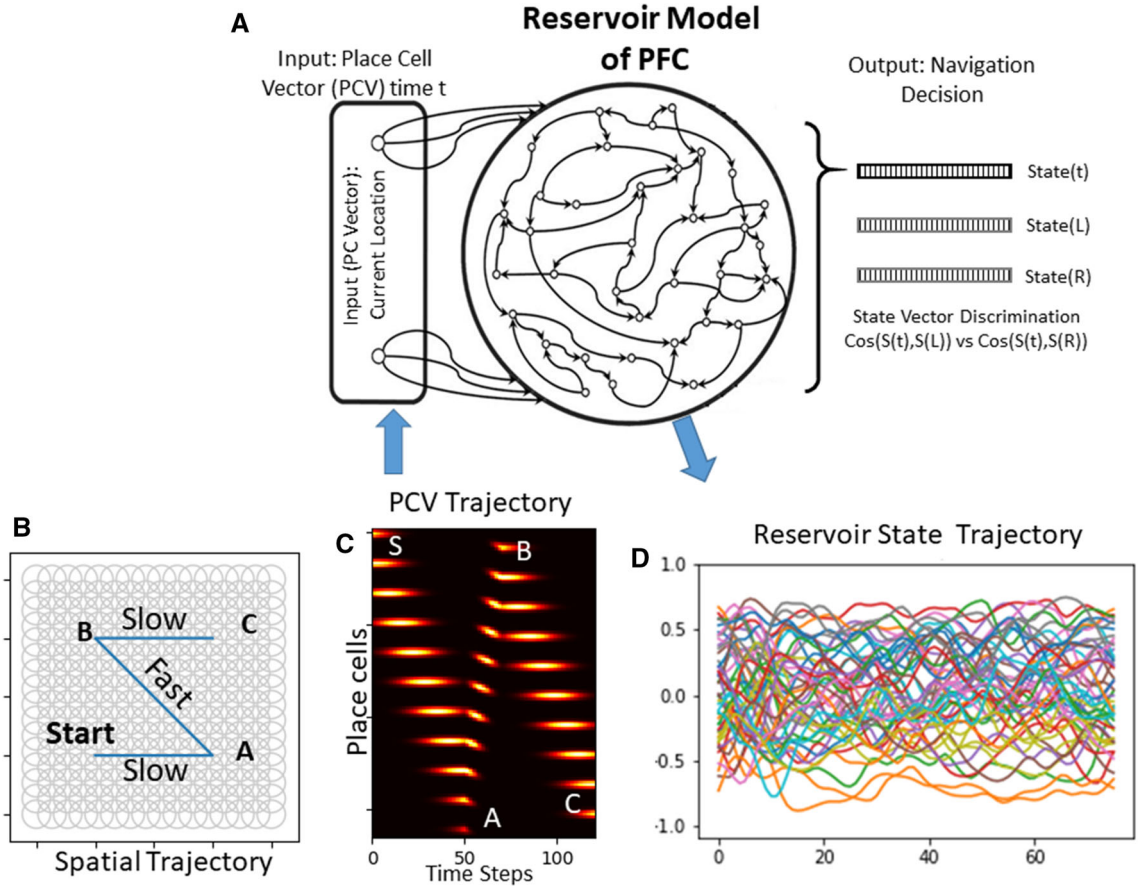

Fig. 1 System Overview. **A** The reservoir model of PFC receives place cell vectors as input. Speed is implicitly coded in the input trajectory. Behavioral output as discrimination choice by comparing reservoir state to "learned"/stored states arising from distinct training trajectories. **B** Overhead view of a spatial trajectory, with 256 place fields overlaid in a 16 × 16 grid. **C** Temporal view of place cell activation vectors. The heatmap illustrates the activity of all the 256 place cells for the trajectory shown in B. Each column shows the place cell vector for the respective time, while each row shows the activity of a single cell through time. Note how the speed of the animal is implicitly coded in the plot by observing the shorter, steeper slope for segment AB (where the rat moves fast) than SA and BC (where the rat moves slowly). **D** Activation of a subset of reservoir-PFC neurons in response to the input sequence of place cell activation vectors (PCVs)

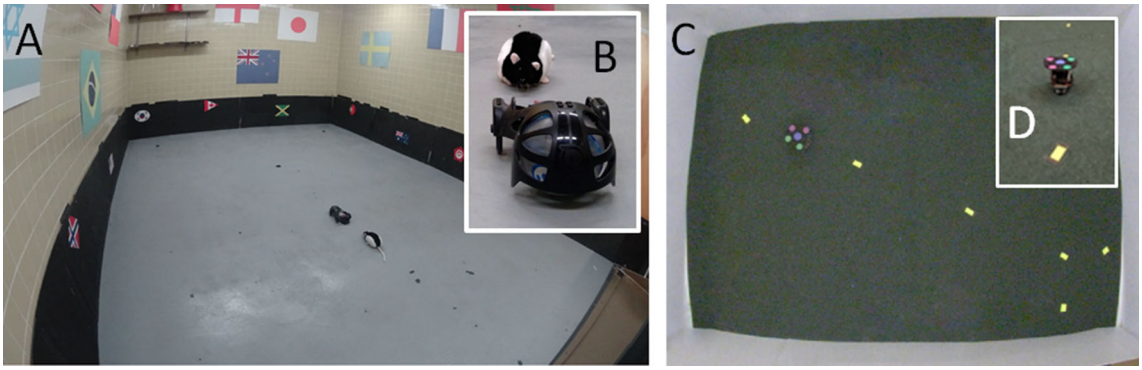

Fig. 2 **A** Rat megaspace environment. Note the large open space, with the Sphero robot leading the rat. **B** Detail of rat with the Sphero guiding robot. **C** Robot environment containing markers for spatio-temporal trajectories. The Raspberry Pi-based robots were designed and built at the USF Biorobotics Lab. Place cell activations for the current article were driven by the overhead camera that uses the five circular color markers on top of the robot to track its location. **D** Robot details

differential drive mobile robot experimental work comparable to the rat experiments to evaluate the computational models. Finally, in order to better understand the underlying neural representations, we compare the coding features of our reservoir-PFC model to those of a set of linear integrators. Linear integrators serve as an appropriate control model as they have been used to model temporal processing in the cortex but do not employ recurrent connections between neurons (Chien & Honey 2020; Huk & Shadlen 2005). The open-space environments for rats and robots are illustrated in Fig. 2.

As a result of our experimentation, our models generate predictions about how: (1) Modifications of the temporal structure of a navigation sequence change the properties of neuronal activity in the PFC (revealed by mixed spatial/temporal selectivity); and (2) Selective manipulations of the temporal profile of spatial navigation (e.g., speed) allow the rat to discriminate between identical spatial trajectories. Importantly, our comparison between the reservoir-PFC model and the linear integrator makes predictions about the neural coding that should be found in the rat PFC. Additionally, we conclude that, while both models can solve the spatio-temporal task, reservoir units display a form of mixed selectivity that is highly reduced in the linear integrator. This is important because linear integrators have been suggested as models of temporal integration in the cortex (Chien & Honey 2020; Huk & Shadlen 2005). Thus, the mixed selectivity profile that may someday be observed in the rat cortex can be compared with these models that are dissociated by their mixed selectivity profiles.

In the remainder of this article, Sect. 2 presents related work, Sect. 3 presents the HIPP-PFC model, Sect. 4 presents the experiments and results, and Sect. 5 presents general conclusions and discussions.

2 Related work

2.1 Reservoir computing

Reservoir computing refers to a class of recurrent neural network models in computational neuroscience and machine learning (reviewed in (Lukosevicius & Jaeger 2009)). Such models are characterized by sparsely connected recurrent networks of neurons with *fixed* connection weights (excitatory and inhibitory). Because of the recurrent connections, this "reservoir" is a dynamic system with inherent sensitivity to the serial and temporal structure of input sequences (Buonomano & Laje 2010; Dominey 1998a, Dominey 2000). Reservoir neurons are connected to readout neurons by modifiable connections that can be trained in different tasks (e.g., sequence recognition, prediction, classification). A first instantiation of reservoir computing modeled prefrontal cortex as a network of leaky integrator neurons with fixed recurrent connections, and modifiable readout connections corresponding to the corticostriatal projections with dopamine-modified synapses (Dominey et al 1995). Buonomano and Merzenich (Buonomano 1995) developed a related model implementing a neural temporal to spatial transformation based on a dynamic state that was sensitive to the temporal structure. Maass et al. (2002) developed a related approach with a recurrent neural network and demonstrated the nonlinear computational capabilities of these systems. Jaeger and Haas (Jaeger 2007) demonstrated how such reservoir systems had inherent signal processing capabilities. When properly exploited, recurrent dynamics can provide an inherent and robust representation of time (Buonomano & Laje 2010; Dominey 1998a). In sensorimotor sequence learning, these models demonstrate inherent sensitivity to serial and temporal structure in motor behavior and language (Dominey 1998a, b, Dominey 2000, Hinaut 2013).

Interestingly, when these networks are exposed to inputs with multiple dimensions (e.g., target identification, serial order, match/non-match), neurons represent nonlinear mixtures of these dimensions (Dominey et al 1995; Rigotti et al 2013). Such nonlinear mixed-effects have subsequently been robustly demonstrated experimentally in the primate frontal cortex, with reservoir activity being highly predictive of neural activity in various cognitive tasks (Enel et al 2016; Fusi et al 2016; Rigotti et al 2013).

Although existing research has examined mixed selectivity in cortex and reservoir networks using tasks that had a succession of stimuli and responses (Enel et al 2016; Rigotti et al 2013), the temporal structure of these sequences was never systematically manipulated to determine how was the temporal structure itself included in the high-dimensional mixed selectivity of individual neurons.

2.2 Spatio-temporal sequence learning in rats

Research in rats has shown that deliberative spatial navigation involves a close interaction between the hippocampal formation and the medial prefrontal cortex (reviewed in (Dolleman-van der Weel 2019; Schmidt et al 2019)). The vast majority of studies of the neural substrate of spatial navigation in rodents are conducted in spatially restricted environments, using simple tasks (e.g., T-maze, Morris water maze). In most of these tasks, the completion time of a trial is passively observed and used to measure performance. A few studies have attempted to control the speed of movement, but only in artificial apparatus, e.g., treadmills or virtual reality (Aghajan 2015, Furtunato 2020, Kraus et al 2013). While much has been learned about the influence of speed on basic cells properties in the hippocampus and entorhinal cortex (Góis & Tort 2018; Iwase et al 2020), there is still very little known about its influence on PFC during navigation, especially as an information channel for learning (i.e., *using speed as a cue to decide where to go next*). Current theories posit that space and time may not be explicitly represented in the brain but dynamically constructed (Buzsaki & Llinas 2017). This construction in the rodent requires active movement such as spatial navigation or internal self-organized reverberations, such as observed during the phenomenon of awake replay (Eichenbaum 2014; Pastalkova et al 2008). The constructed (and hence subjective) nature of the space–time relations is well-documented in humans: The perception of time is accelerated during pleasurable experiences and slowed during negative ones, a phenomenon possibly dependent on the dopaminergic system (Honma 2016). Importantly, the recall of distance actually traveled can be significantly underestimated and compressed depending on the complexity of the paths navigated (Bonasia 2016). The hippocampus has been well characterized in terms of its ability to exhibit multi-modal ordinal sequences of activities (Buzsaki & Llinas 2017). However, the extent to which this property depends on the equally well-documented sequence generation property of the PFC is unknown. The most common manner by which space and time are related in spatial navigation is through the assessment of speed. It was shown, for example, that speed could be "read out" from the theta-phase and firing rate of a place cell as the rat crosses its field (Geisler 2007; McClain et al 2019). However, these a-posteriori assessments are mostly correlative and do not give insights into the actual function of speed on a trial-by-trial basis. Such an understanding can be best obtained by *precisely controlling the speed of the rat on a trial-by-trial basis* and measuring the effect of this manipulation on behavior and neural activity. Seminal lesion studies have shown that temporally spacing items facilitate recall in rat spatial navigation. Lesions of the hippocampus impair recall at all spacing intervals, while lesions of the prefrontal cortex produce a gradual impairment (the longer the interval, the smaller the impairment) (Chiba 1994). These results clearly suggest that both PFC and HIPP are involved in temporal sequence learning, but that they may have different roles.

Recent work has shown a novel method that allows natural and efficient control of rat trajectories and speed in open megaspaces. A robot can guide a rat in a complex multi-goal maze to learn a path to reach a specific goal using only one robot-guided demonstration trial (Gianelli 2018). In separate experiments, it was also shown that rats could be trained to precisely follow the robot at specific speeds and in specific directions in a sustained and robust manner and that following a robot yielded similar place cell firing patterns as in classical navigation experiments (Gianelli 2018).

2.3 Spatio-temporal sequence learning and evaluation with robots

Physical robotic systems have played an important role in evaluating hippocampus computational models under realistic and uncertain conditions. Examples of place cell models evaluated with physical robots include works by (Arleo 2000; Caluwaerts 2012; Filliat 2002; Milford & Wyeth 2010; Barrera 2008, 2010, 2011, 2015; Llofriu 2019, 2015; Scleidorovich 2020; Tejera 2013, 2015, 2018). Examples of sequence learning reservoir models evaluated with physical robots include works by (Cazin 2019, 2020; Hadi Salman et al 2018; Tekülve Jan et al 2019). In the current paper, we provide an evaluation of spatio-temporal integration with a physical robot.

3 HIPP-PFC model

In this article, we hypothesize that reservoir networks can simulate the PFC's ability to generate high-dimensional representations of their inputs, revealed by mixed spatial and temporal selectivity. As such, our model consists of two components: the reservoir-PFC model itself and a hippocampal place cell model that simulates noisy place cell activity used as input by the reservoir. The details of each model are described in the following subsections. Additionally, we also describe an alternate PFC model that uses a linear integrator instead of the reservoir. This alternate model is used as a control to compare the reservoir results with a system that performs temporal integration with no between-neuron recurrent connections (in the sense that integrator neurons do not depend on other integrator neurons as in the reservoir). It is a reasonable model for comparison, as linear integrator models have been proposed to account for spatio-temporal integration in the cortex (Chien & Honey 2020; Huk & Shadlen 2005).

3.1 HIPP–Place cells model

The noisy activity of place cells was modeled using Gaussian kernels, as shown in Eq. 1. The equation calculates the activity of a place cell by applying the kernel to the distance between the rat's position and the place field center while adding two noise sources.

$$P_i(\mathrm{t}) = e^{-\left(\frac{\left|\left|\vec{x}_t - \vec{x}_i\right|\right|(1+\epsilon_i(t))}{\sigma}\right)^2} + \epsilon_i^{'}(t) \tag{1}$$

where $P_i(t)$ represents the activity at time t of a place cell i with field center at $\vec{x}_i$. The position of the rat at time t is given by $\vec{x}_t$. The Gaussian's standard deviation σ (set to 0.1679) controls the size of the place field. Additionally, random variables $\epsilon_i(t)$ and $\epsilon_i^{'}(t)$ model the two noise sources for place field i at time t. The first variable simulates a cell's localization error by adding an extra factor in the calculation of the distance between the rat's position and the place field center. This factor adds or subtracts a percentage of the distance's original value. The second variable simulates noise in the overall output of place fields, denoted as "additive noise." In contrast to the former, the noise to signal ratio of additive noise can be very high as its intensity is independent of the place cell's activity. In our experiments, random variables $\epsilon_i(t)$ and $\epsilon_i^{'}(t)$ were sampled from uniform distributions with ranges $[-u, u]$ and $[-u', u']$, respectively, where u and $u^{'}$ are two parameters that control the noise intensity and vary with the experiments. To exemplify how noise affects place cell activity, appendix Fig. 12 presents a table of heatmaps illustrating the activity of place fields along a predefined path for different values of u and $u^{'}$.

3.2 PFC–Reservoir model

We model the PFC using the basic discrete-time, tanh-unit, echo state network with N reservoir units and K inputs characterized by the state update shown in Eq. 2.

$$\vec{x}(t+1) = (1-\alpha)\vec{x}(t) + \alpha f\left(W\vec{x}(t) + W_{in}\vec{P}(t)\right) \tag{2}$$

where $\vec{x}(t)$ is the N-dimensional reservoir state at time t, f is the $tanh$ function, α is the leak rate, W is the $N \times N$ reservoir weight matrix, W_{in} is the $N \times K$ input weight matrix, and $\vec{P}(t)$ is the K-dimensional vector of place cell activities computed at time t according to Eq. 1. The matrix elements of W and W_{in} are drawn from a random distribution and are not modified in time. Additionally, place cell activity was computed according to Eq. 2.

The reservoir was instantiated using "easyesn," a python library for recurrent neural networks using echo state networks (https://pypi.org/project/easyesn/) (Thiede & Zimmermann 2017). The input was a 256-element vector. In experiments 2 and 3, we used reservoirs with 400 neurons. In experiment 4, the reservoirs had 256 units to allow direct comparison with the 256-element leaky integrator. Input dimensions correspond with the 16 × 16 grid of place cells represented as a 256-element vector. The $\boldsymbol{W}$ and $\boldsymbol{W_{in}}$ matrices were initialized using a uniform distribution ranging from − 0.5 to 0.5. The leak rate was set to 0.05 based on our empirical observations and the high volatility of the input. The leak rate influences the memory delay capacity of the system, with smaller leak rates corresponding to slower fading of past influences. In all experiments, the reservoirs are initialized to a nonzero activation state by feeding the network with a predefined PC activation sequence (see pseudocode Table 3 lines 13 and 19).

Note that although reservoir computing typically models the decision processes by training the reservoir's output layer to harvest the rich high-dimensional reservoir states (Lukosevicius & Jaeger 2009), we are instead focused on analyzing the reservoir states themselves and, thus, we do not use nor train the reservoir's output layer. Instead, we follow an approach similar to (Bianchi et al 2020), where the reservoir states were used as input to a vectorial data classification algorithm. Following this approach, we model the rat decision process using this method and a simple cosine similarity classification algorithm described in Sect. 4.4.1. Such a discrimination task could also be implemented by training readouts to respond to the two respective choices.

3.3 PFC–Linear integrator model

To compare the reservoir with a model that performs spatio-temporal integration with no between-neuron recurrent connections, we compared the model with a linear integrator with 256 neurons (one neuron per place cell). Such linear integrators have been used to model temporal processing in the cortex (Chien & Honey 2020; Huk & Shadlen 2005). The integrator is specified in Eq. 3. Note that, as opposed to the reservoir, there are no connections between integrator neurons.

$$L_i(t) = \begin{cases} (1-\alpha_i)L_i(t-1) + (1+\alpha_i)P_i(t) \; if t > 0 \\ P_i(0) \; if t = 0 \end{cases} \quad (3)$$

We previously used this integrator model as a control for comparison with reservoir simulation of human cortical activity during narrative processing (Dominey 2021). In our current experiments, we used two versions of the linear integrator model. One version uses constant leak rates, while the other uses variable leak rates. The constant model sets α_i to 0.05 for all neurons. On the other hand, in the variable model, each α_i is independently drawn from a uniform distribution with range [0, 0.1]. Note that the constant linear integrator can be considered a particular case of the variable linear integrator where all leak rates are set to the uniform distribution's expected value. As in the reservoir, the leak rate influences the retention of past inputs, with smaller leak rates corresponding to longer retention.

4 Methodology, experiments, and results

4.1 Overview

The current article presents 4 experiments that progressively assess our hypothesis. The experiments are summarized in Table 1. In experiment 1, we first test whether rats can indeed use their running velocity as a factor for making navigation decisions. Given this evidence, in experiment 2, we determine whether a PFC reservoir model could be used to make navigation speed discriminations. Given this infrastructure, in experiment 3, we use a differential drive robot to assess the model with more realistic trajectories. While experiments 1–3 examine the behavior of the rat and the PFC-reservoir system, experiment 4 examines the neural coding underlying this behavior, focusing on mixed selectivity. Thus, experiment 4 analyzes mixed selectivity (the interaction between location and speed profile) in the PFC-reservoir and in a functionally similar linear integrator model that integrates space and time. The difference between the neural coding in these models thus poses a challenge to future neurophysiological experiments that can dissociate between these two models.

4.2 Experiment 1—Speed profile discrimination in rats

This exploratory experiment examined whether rats could be trained to discriminate between different temporal structures of navigation (i.e., different speed profiles) imposed over the same spatial path by following a robot. This exploits a novel capability to control rat trajectories in terms of spatial path and velocity (Gianelli 2018; Harland et al 2021). To our knowledge, no experiment in open space has been conducted to test such a hypothesis, so these experiments are aimed at testing the feasibility of the paradigm. Can a rat use speed as an information channel to make a spatial navigation decision in megaspace? If so, we are motivated to understand how speed might be represented in a computational model of PFC.

4.2.1 Methods

We used four 5–7 months old male (3) and female (1) Brown Norway rats. Rats were trained to navigate on the floor of a large 5.3 m × 3.5 m room ("megaspace"), configured for spatial navigation experiments (Harland et al 2021). The room has a rough washable floor and several overhead cameras to track the movement of the animals. Rodents were pre-trained to follow a small mobile robot controlled by the experimenter, as previously demonstrated (Gianelli 2018). The robot carried a light that was on when in action and off when the rat was encouraged to continue without the robot. The robot pulled a small cart that contained a 20 mg food pellet. Rats were pre-trained to follow the robot at random speeds around the room for 2–3 weeks.

In a series of spatio-temporal discrimination experiments, we trained rats in the megaspace to follow the baited robot at either slow (30 cm/s) or fast (55 cm/s) speeds, consistently mapping one speed with either one of the two arms of a Y pattern (no walls, open field, guided learning trials, ten trials per side, pseudo-randomly ordered, each branch of the Y pattern was 1.1 m long, the stem was 3 m long). These speeds were

Table 1 Experiment summary. The table summarizes the subjects used in each experiment and the experiment's objective

Experiment	Subject	Objective summary
1	Rats	Can rats discriminate between speed profiles?
2	Simulated	Can reservoir discriminate between speed profiles?
3	Robot	Can reservoir discriminate realistic robot trajectories?
4	Simulated	Assess neural coding and compare to linear integrators

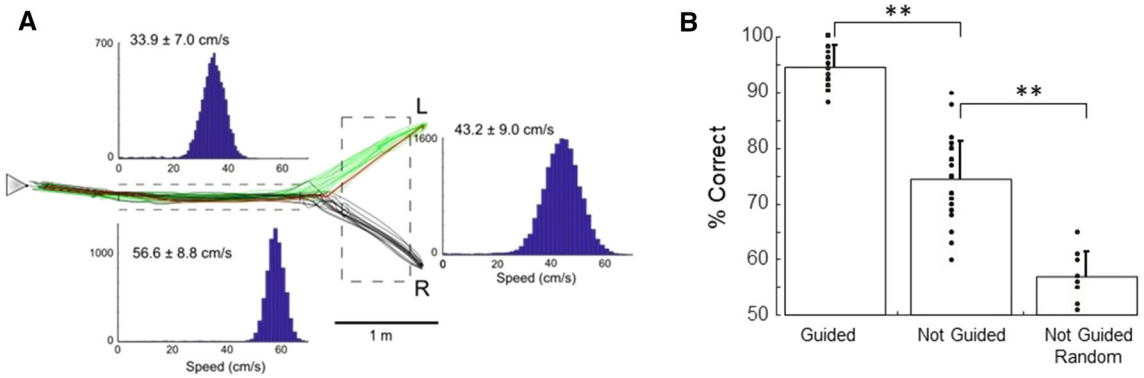

Fig. 3 Speed is an effective cue for spatial decision-making. **A** Trajectories of the rat are shown for test trials after the rat learned that slow stem speed was associated with left choices (green) and fast stem speed was associated with right choices (black). Trajectory: 1 session, 30 trials. 1 error (red). Speed histograms: 1 rat, 7 sessions. Speeds for slow (33.9 cm/s) and fast (56.6 cm/s) are significantly different ($p <$ 0.001). The third histogram shows the speed of the non-guided rat on the two arms (no difference between R and L, so data were combined). **B** Overall performance during guided training trials, non-guided test trials (as in A), and non-guided test trials following random side-speed guided pairing (4 rats, 27 sessions). Statistical tests were ANOVA with Bonferroni correction (**p < 0.01)

chosen experimentally so that the animal's gait was similar in the two conditions (fast walking, no galloping). This ensured that the gait itself was not a cue for decision-making. Food cups were positioned at the end of each arm. During learning, the rats were given 20 pseudo-randomly ordered trials (e.g., 10 trials slow speed to the left arm, 10 trials fast speed to the right arm). The correct arm of the Y maze contained a food pellet. During test trials, the robot stopped at the decision point (end of the stem); the rat consumed the bait from the robot and then had to choose between continuing by itself left (green traces, Fig. 3A) or right (black traces), depending on the speed experienced on the stem (pseudo-random test order). The distribution of instantaneous guided rat speeds in the stem across seven sessions (horizontal dashed box) is shown for left trials (top) and right trials (bottom). We note here that the use of a megaspace to study the influence of speed patterns on decision-making is crucial because small spaces do not allow navigating at sustained/constant speeds for long enough distances. In small spaces, desired speeds can only be reached transiently.

4.2.2 Results

The right histogram (Fig. 3A) shows the speed of the non-guided rat on the two arms (no difference between R and L, so data were combined, vertical dashed box, speed 43.2 ± 9.0 cm/s). The rat made one error out of 30 trials in this session (red). Across four rats (three males, one female) and 27 sessions, rats reliably followed the robot during learning (Fig. 3B, Guided) and reached over 74% correct during testing (Not-Guided), showing that speed information on the common stem alone was an effective cue for spatial decision making. In additional experiments where rats were given guided trials in which speed and side were unpaired, rats behaved randomly (Not Guided Random), with a slight preference for the left arm (not shown). Statistical tests were ANOVA (linear model with Gaussian noise), Bonferroni corrected (**p < 0.01).

4.3 Experiment 2—Speed profile discrimination by the PFC-reservoir

Experiment 1 demonstrated that rats are sensitive to velocity, which thus motivates us to ask how speed might be represented in a recurrent model of PFC. This experiment aims to determine if the PFC reservoir model can generate spatio-temporal representations that can distinguish between different navigation trajectories that cover the same spatial path but different temporal structures.

4.3.1 Methods

Experiment 2 tests the ability of the model to discriminate between navigation trajectories 4A and 4B, as illustrated in Fig. 4. Both trajectories use the same amount of time to traverse the same path through points "Start," "A," "B," "C," and "D." The only difference between 4A and 4B is the temporal structure, which refers to the speeds used to navigate each segment.

The goal of the experiment is to determine whether the two instances of a reservoir that reached D after temporal structure 1 (Med, Fast, Slow, VFast, 4A) vs. temporal structure 2 (Med, Slow, Fast, VFast, 4B), will exhibit significantly different states to allow discrimination so that the system could learn to go left after temporal structure 1 and right after temporal structure 2. The specific temporal structures

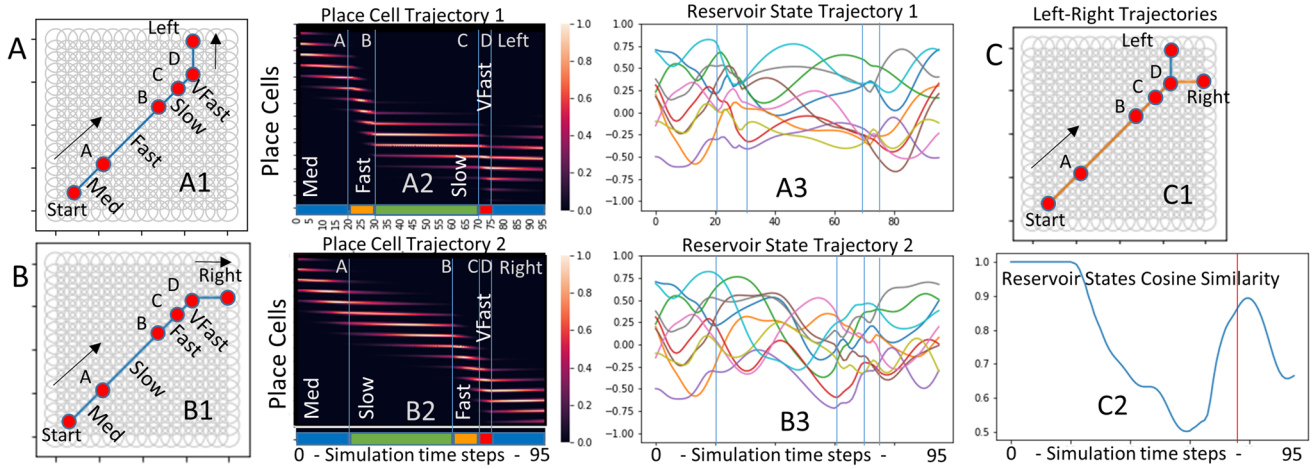

Fig. 4 PFC-reservoir model evaluation in a speed-position discrimination task. Simulated rats must follow the straight path Start-ABCD with two different temporal structures (shown in rows A and B). At point D, rats must turn either left (row A) or right (row B) based on the temporal structure used. **A** Temporal structure 1 (TS1). **A1** Spatial path ABCD 16 × 16 place cell field, with different velocities. **A2** 256 place cells (v-axis) over time (h-axis). Segment Start-A is medium speed (blue), AB is fast (orange) and short in duration, BC is slow (green) and longer in duration, CD is very fast, etc. **A3** 10 of 400 reservoir unit activations driven by this place cell trajectory input. **B** Temporal structure 2. **B1** Same as A but with a different temporal structure, associated with a right turn. **B2** Note: AB is much longer in time and slower (green) than in TS1. TS1 and TS2 differ in the durations (thus velocities) of AB and BC. **B3** Activations of same reservoir units as in A3. Note the difference with A3. **C1** Left–Right Y paths. **C2** Cosine of reservoir activation vectors for A3 and B3. Starting at the difference in velocity for AB, the cosine indicates reservoir states are distinct. The red vertical line indicates where the reservoir activity must be used to discriminate between TS1 and TS2 to turn left or right. When cosine < 1, discrimination is possible

Table 2 Temporal structures 1 and 2 start and end with the same speeds. Ending with the same speed means that discrimination at D cannot be based solely on the latest speed but requires more memory instead

	Start–A	A–B	B–C	C–D
Temporal structure 1	Med	Fast	Slow	VFast
Temporal structure 2	Med	Slow	Fast	VFast

used are shown in Table 2. Importantly, to prevent discrimination based solely on final speeds, both trajectories share the same final speed, which forces the network to remember older speeds.

To assess the model, each trajectory is transformed into a trajectory of place cell activations over a 16 × 16 place cell grid, as illustrated in Fig. 4A2 and B2. We observe that in the initial segment for both trajectories, the displacement from Start to A is at medium velocity (Med) and that the place cell coding in both cases is identical. In trajectory 1 (panel A), the following segment from A to B is performed fast, seen in Fig. 4A2 as a rapid change in the activation pattern in the subpanel labeled fast. In contrast, for navigation trajectory 2, this segment from A to B is navigated slowly. This is seen in Fig. 4B2 as a slower change in the place cell activation pattern in the subpanel labeled slow. The segment from position B to C is slow for trajectory 1 and fast for trajectory 2. Both trajectories arrive at C at the same time. Finally, the segment from C to D is very fast for both, which ensures that any discrimination capability will not be due to simply keeping track of the final velocity. Panels A3 and B3 display the activation for a subset of PFC reservoir neurons in response to these two place cell trajectories. In this form, it is hard to appreciate the difference in patterns. Thus, to evaluate the discrimination capability, we measured the cosine between the two PFC reservoir activation vectors after reaching point D, where the decision must be made to turn left for temporal structure 1 (Fig. 4A) and right for temporal structure 2 (Fig. 4B).

4.3.2 Results

Figure 4C2 displays the cosine similarity between the internal states of two identical reservoirs as they are exposed to the two temporal structures. We can observe that, initially, where the two trajectories are identical, the cosine similarity for the internal states is at its ceiling of 1. Note that in this experiment there is no noise in the place cell coding. Then, as we transition from A to B at different speeds, the reservoirs exhibit a marked cosine similarity difference (cosine < 1) (see place cell trajectories in Fig. 4A2 and B2). Likewise, the transitions from B to C are at different speeds for the two

navigation trajectories. Finally, the transition from C to D is the same for both. Importantly, at the crucial moment, when the simulated rat is at point D (the decision point, vertical line), the cosine between the two PFC-reservoir unit vectors remains significantly different from 1, indicating that even though the trajectories were identical at this point, the different speed patterns generated different network states.

4.4 Experiment 3—Speed profile discrimination by a robot with PFC-reservoir

Experiment 2 showed how the reservoir can generate state vectors that distinguish between different place cell trajectories. Experiment 3 uses a real robot to generate a dataset of trajectories to evaluate the PFC-reservoir's ability to discriminate different speed profiles in more realistic circumstances.

4.4.1 Methods

Unlike experiment 2, which used synthetic trajectories with highly contrasting speed profiles that favored the discrimination task, experiment 3 used a differential drive robot to generate a dataset of realistic trajectories used to perform offline classification.

As illustrated in Fig. 5A and B, experiment 3 had the robot navigate a straight line composed of 3 equal segments using temporal structures SFS (slow, fast, slow) and FSS (fast, slow, slow). As in experiment 2, the temporal structures indicate the speeds for traversing each segment, and they were chosen so that the final speed and the overall duration remain the same, making speed patterns the only discriminating factor between both temporal structures.

While navigating, the robot's position was recorded every second using an overhead camera, and the resulting trajectories were tagged with the sequence name and then stored to create a dataset. In total, we recorded 60 trajectories (30 of each type), each covering approximately 240 cm. Speeds were set to 8 and 12 cm/s for slow and fast segments, respectively, yielding an overall average speed of 9 cm/s. Each segment is approximately 80 cm. Note that speeds and distances are only an approximation, as the robot's motion is subject to noise.

After recording the trajectories, the resulting dataset was divided into 15 subsets used to simulate 120 rats (8 rats per subset) in a sequence classification task. Each subset consisted of 4 trajectories (2 of each type), and different rats used different random seeds (affecting the reservoir initialization and place cell noise). The classification task required simulated rats to use one set of prerecorded paths as input to the model and to generate the 4 final reservoir states for the four respective trajectories. After generating the states, 2 states (one of each sequence type) were used to instantiate a nearest-neighbor classifier, while the other 2 were used to evaluate it. Distance between states was measured using the cosine similitude between vectors. Table 3 shows the complete pseudocode for the experiment.

This classification method which discriminates reservoir states at sequence completion is functionally equivalent to a set of readout neurons trained to activate for left or right, and allows efficient analysis of the reservoir state differences.

4.4.2 Results

To assess the reservoir's robustness in the robot classification experiment, the experiment was repeated 25 times for different noise configurations varying u and u' (the localization and additive noise levels from Eq. 1) from 0 to 0.4 in increments of 0.1.

During the discrimination task without noise (u and u' set to 0), the robot-reservoir system always misclassified the same prerecorded trajectory despite the different seeds. To assess whether other factors may have influenced the decision process, we reviewed whether all recorded sequences had approximately the same duration. Due to mechanical variability in the path execution, some of the testing trials with the FSS sequences were significantly longer than others. This variability is usually due to friction between robot wheels and the floor, particularly at slow speeds. To verify that this did not create an artifact that might facilitate the task for the reservoir, trajectories were re-recorded after applying a filter based on space. Originally, positions were sampled every second, but the added filter removed samples if the robot moved less than 2 cm from the last recorded position, thus shortening the sequence. Under these conditions, the 60 recorded sequence executions had 24.55 data points on average. To assess if there was no significant difference after filtering, we performed a Kruskal Wallis H test comparing the lengths of each sequence type and stage (i.e., the training and testing stages of the nearest neighbor classifier). Results are illustrated in Fig. 5C and show no significant difference in the rank sums of the four groups ($H = 3.68$, $p = 0.298$). Using these data, which reduces the bias due to different sequence lengths, the system now performed at 100% correctness in the zero-noise condition. That is, the resulting reservoir state of each test sequence had a higher cosine similarity to the reservoir state for its matching sequence than its non-matching sequence. This difference was highly significant ($t = 120$, $p = 1.3e-233$), as illustrated in Fig. 6.

Figure 6 shows results using the filtered paths for 3 sample noise configurations (see appendix Figs. 12 and 13 for all noise levels). Results show that the reservoir could tolerate combined noise levels of up to 10% without decreasing accuracy. Additionally, the effect of localization noise on the accuracy was very small. Particularly, the differences observed by varying the localization noise seem to be due to the variability of the additive noise. On the other hand,

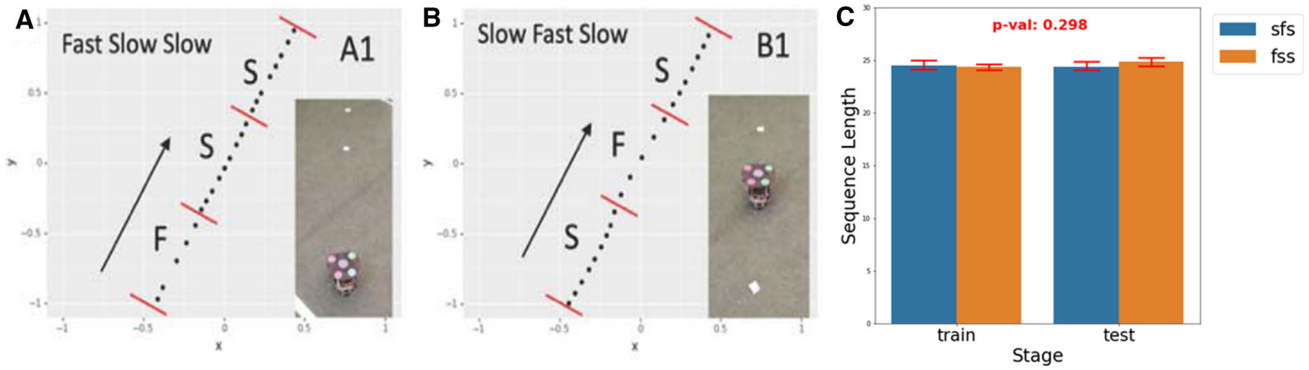

Fig. 5 Two of the sixty robot trajectories recorded for the robot experiment. **A** Fast-Slow-Slow. **B** Slow-Fast-Slow. These trajectories covered ~ 240 cm with an average speed of ~ 9 cm/sec. **C** Robot sequence lengths after applying the filter. The image shows bar plots of the number of points in each sequence grouped by sequence type and the stage in which they were used (i.e., for "training" the nearest neighbor classifier or for testing it). The red number on top shows the p value resulting from applying a Kruskal–Wallis H test to the four groups

Table 3 Pseudocode for simulating rats from real robot trajectories

```
1   // use the robot to generate trajectory data set
2   data_set = {}
3   repeat 30 times:
4       for sequence s in [ SFS , FSS ]:
5           path = perform s with robot and record positions.
6           data_set.append(path)
7   subsets = divide data_set into 15 subsets each with 2 SFS and 2 FSS sequences
8
9   // simulate 120 rats (8 rats per subset):
10  for subset in subsets:
11      repeat 8 times:
12          set new random seed
13          instantiate reservoir, use a predefined sequence as input and save state
14
15          // Calculate final reservoir state for each path
16          states = {}
17          for path p in subset:
18              A = calculate noisy PC activations of p
19              restore reservoir state from line 13 and use A as input
20              r_p = get internal reservoir state
21              states.append(r_p)
22
23          // classify using nearest neighbor
24          let states = {r_SFS1, r_SFS2, r_FSS1, r_FSS2} be the result from lines 16-21
25          for r in {r_SFS2, r_FSS2}:
26              prediction = argmax {cos(r, r') for r' in {r_SFS1, r_FSS1}}
```

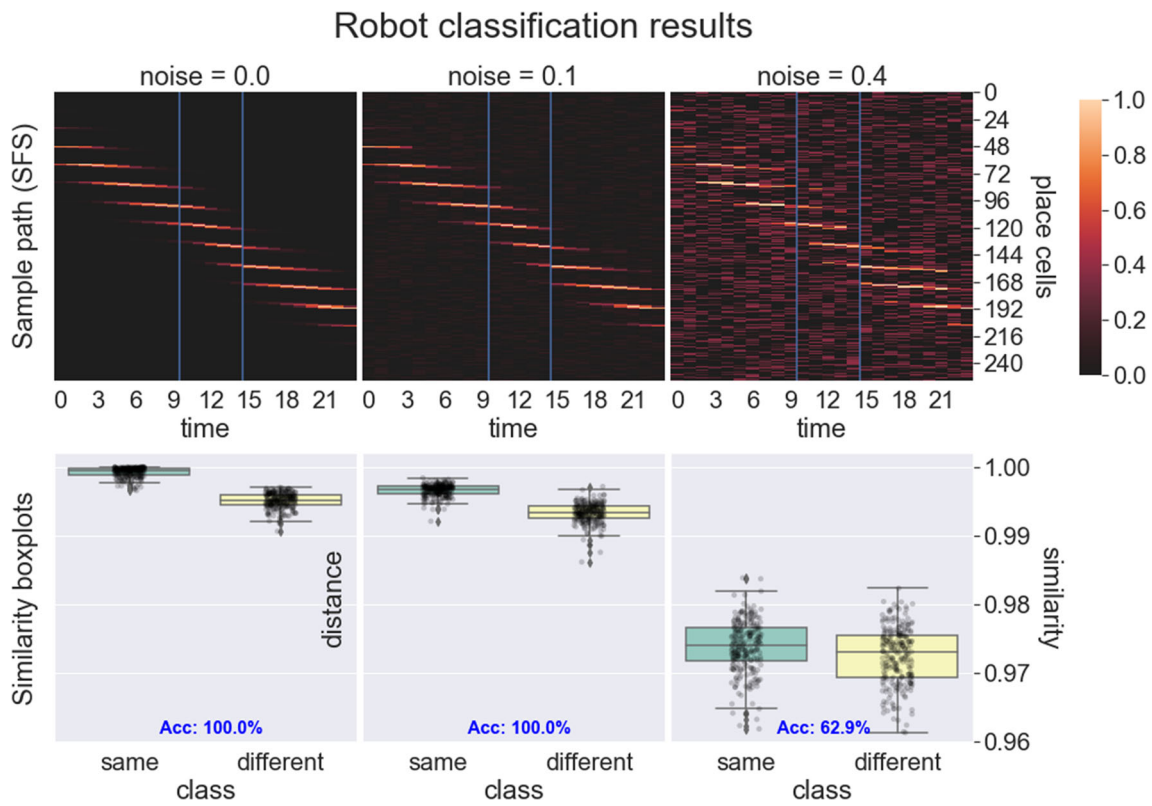

Fig. 6 Robot classification results. Experiment 3. The image above shows the classification results from the robot experiments for 3 different noise levels indicated by each column using the same level of additive and localization noise. The heatmaps on the first row illustrate the noisy PC activations for a sample SFS traversal. Vertical blue lines indicate the three segments in the trajectory. The box plots on the bottom illustrate the distributions of cosine similarities between instances of the same and different classes (sequence types). The blue number at the bottom indicates the accuracy obtained by the nearest neighbor classifier for the respective noise level

additive noise had a more significant effect. When averaging results, additive noise reduced the accuracy by 6.18% when using 20% noise, 24.18% when using 30% noise, and 35.42% when using 40% noise. Although reductions of 24.18% and 35.42% are very significant, we must note that this was achieved at 30% and 40% combined noise, which is very high for a computational system. Figure 7 illustrates sample executions of a reservoir instance on the SFS and FSS robot sequence trajectories. Panel E shows the cosine similarity between the reservoir inputs (i.e., place cell vectors) of both trajectories. There we see that the place cell representations of the two sequences are indeed different during the initial two segments but then converge in the third segment, which is slow (S) for both. Interestingly, as observed in panel F, which shows the cosine similarity for reservoir states, the network maintains sufficient memory of the past to retain the difference between both sequences.

We evaluated the discrimination performance systematically, varying the localization and additive noises between 0 and 0.4 by increments of 0.1, thus yielding 25 noise conditions. The detailed results are presented in appendix Figs. 12 and 13.

The robotic experiments allow us to consider spatial (location) and temporal (speed) noise that are intrinsic to physical robots and caused by, e.g., mechanical variability and ground friction. We evaluated how these aspects affected variability of results, complimentary to the analyses in the purely simulated experiments.

4.5 Experiment 4—Mixed selectivity in the PFC-reservoir and linear integrator

In experiment 4, we assess the reservoir's neural representations, with a particular interest in mixed selectivity, a phenomenon where neurons concurrently encode multiple task-relevant properties, such as space and time (Enel et al 2016; Rigotti et al 2013). Our hypothesis is that, in spatial cognition tasks, the PFC-reservoir will exhibit a high-dimensional neural representation of position and speed profile with mixed selectivity. Experiment 3 already showed that the model could integrate spatial information through time, generating distributed neural representations that could discriminate between different speed profiles. In this experiment, we test the remainder of the hypothesis that

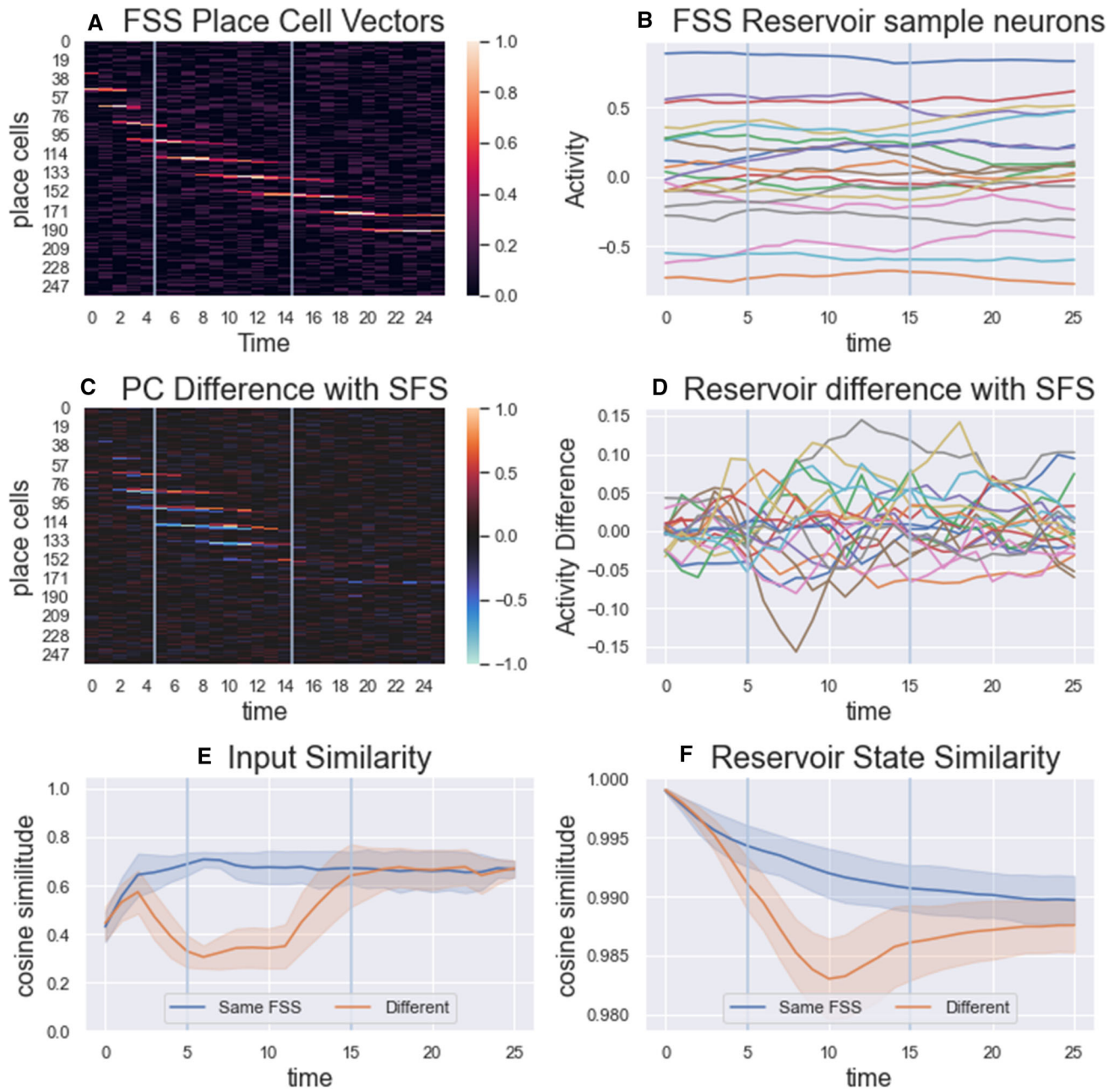

Fig. 7 Experiment 3. PFC-reservoir processing of robot navigation trajectories using 0.2 noise for additive and localization noise. **A** Sample place cell activation trajectory for sequence FSS. **B** Activity of 20 sample reservoir units in response to speed profile FSS. **C** Difference between the place cell activation trajectory of a sample SFS sequence and the sample FSS shown in panel A. **D** Same as C but taking the difference between reservoir activities. **E** Cosine similarity vs. time plots comparing 120 pairs of input sequences (i.e., the vectors of PC activities). The blue plot compares sequences of the same type (FSS), while the red plot compares FSS vs. SFS sequence pairs. Dark lines indicate the mean, while shaded areas indicate the standard deviation. **F** Same information as E but calculates the similarity between reservoir states instead of input states. Note that the distributions of similarities between reservoir states are still different by the end of the sequences, thus allowing the discrimination between sequences. The light blue vertical lines on each plot indicate the three segments of each sequence

the representation will exhibit mixed selectivity for positions and speed profiles.

While we believe that the PFC architecture is reservoir-like (Cazin et al 2019; Dominey 2021; Enel et al 2016; Rigotti et al 2013) based on its massive local connectivity (Ercsey-Ravasz et al 2013; Goldman-Rakic 1987), it is important to compare with alternative models. As stated above, linear integrator models have been proposed to account for spatio-temporal integration in the cortex (Chien & Honey 2020; Huk & Shadlen 2005). The linear integrator model can be built by using a leaky integrator for each of the 256 place cells, with a leak rate that specifies the influence of past inputs on the current state.

4.5.1 Methods

Since we will compare the PFC-reservoir to a 256-element linear integrator, for this experiment, we used a reservoir with 256 neurons for the mixed selectivity analysis. To test mixed selectivity, we should sample the same neuron when the robot is at the same location, at the same time, but in a different speed sequence. Theoretically, these conditions should have been met in the final segments of the robot experimental data, but this was not the case due to stochasticity. Thus, we decided to use new synthetic trajectories to have more control over the experiment.

To assess mixed selectivity, we defined new sequences that ensured testing requirements. These stimuli consisted of 3 sequences of the form FS-FS-FS, SF-SF-FS, and M-M-M. Sequence names indicate the speeds (letter S for slow, F for fast, and M for mean) used to traverse each of the three segments (separated by dashes). Note that all segments of the first two sequences are split into halves. Under these conditions, whether the initial segment is FS, SF, or M, we could guarantee that each of these three speed-segments ends at the same location at the same time.

To assess the number of mixed selectivity neurons of a model, we want to identify the neurons whose activity depends not only on the position but also on the speed profile used to reach that position. Thus, we performed a 3 × 3 ANOVA (linear model with Gaussian noise) for each cell, comparing its activity with factors position and speed, each with three levels corresponding to the three speed profiles (sequence type) and the three positions where place cells were sampled. Neurons were counted as showing mixed selectivity only when the ANOVA speed x position interaction had a p value smaller than 0.01.

To generate sufficient data to assess mixed selectivity at the end of the three segments in trajectories FS-FS-FS, SF-SF-FS, and M-M-M, we replicated each trajectory 20 times, adding ± 2 cm uniform noise to all coordinates in the path except for the final point of each segment. As a result of the data augmentation process, we generated a total of 60 sequences and 180 data points for each place cell (3 data points per sequence). Additionally, we added noise to place cells as in experiment 3, evaluating the same 25 noise configurations.

Mixed selectivity was assessed for 3 different models: a reservoir, a linear integrator with variable leak rates, and a linear integrator with constant leak rates. Note that the first two models depend on the random seed. Thus, we used 10 instances of each model using different random seeds, testing 21 models, including 10 reservoirs, 10 variable integrators, and 1 constant integrator, each with 256 neurons.

In order to observe the relation between mixed selectivity and sequence classification performance, experiment 4 also compares the 3 models in the sequence classification task using the nearest neighbor heuristic on sequences FS-FS-FS and SF-SF-FS as in experiment 3. Unlike the mixed selectivity test, we replicated each trajectory 120 times for classification as the task requires fewer computations.

4.5.2 Results

Figures 8 and 9 illustrate the results of the 256-element reservoir and the 256-element linear integrator on the discrimination task from experiment 4, respectively. As seen in the cosine similarity measures for the two sequences FS-FS-FS and SF-SF-FS, both the LI and the reservoir can discriminate between these sequences. Table 4 shows the number of neurons that had significant effects for each factor. Results show a considerable number of neurons responded to position, speed profile, and, importantly, to the position x speed profile interaction.

Table 4 shows the results of the mixed selectivity analysis for both models. As predicted, the reservoir demonstrated a high proportion (221/256) of mixed selectivity neurons. Interestingly, the LI models also displayed mixed selectivity. To understand these findings, we compared two forms

Table 4 Effects for position x speed profile ANOVA with localization noise 0.1 and additive noise 0.1. Number of neurons/units from 256 that display the effect at $p < 0.01$

ANOVA Effect $p <$ 0.01	Reservoir	V-Integrator	C-Integrator
Main effect: Position	254.5	249.6	250
Main effect Speed profile	219.1	76.3	77
Mixed selectivity: Interaction position × Speed	221.6	63	69
Nonlinear mixed selectivity: P×S with shape change	81.2	5.4	5

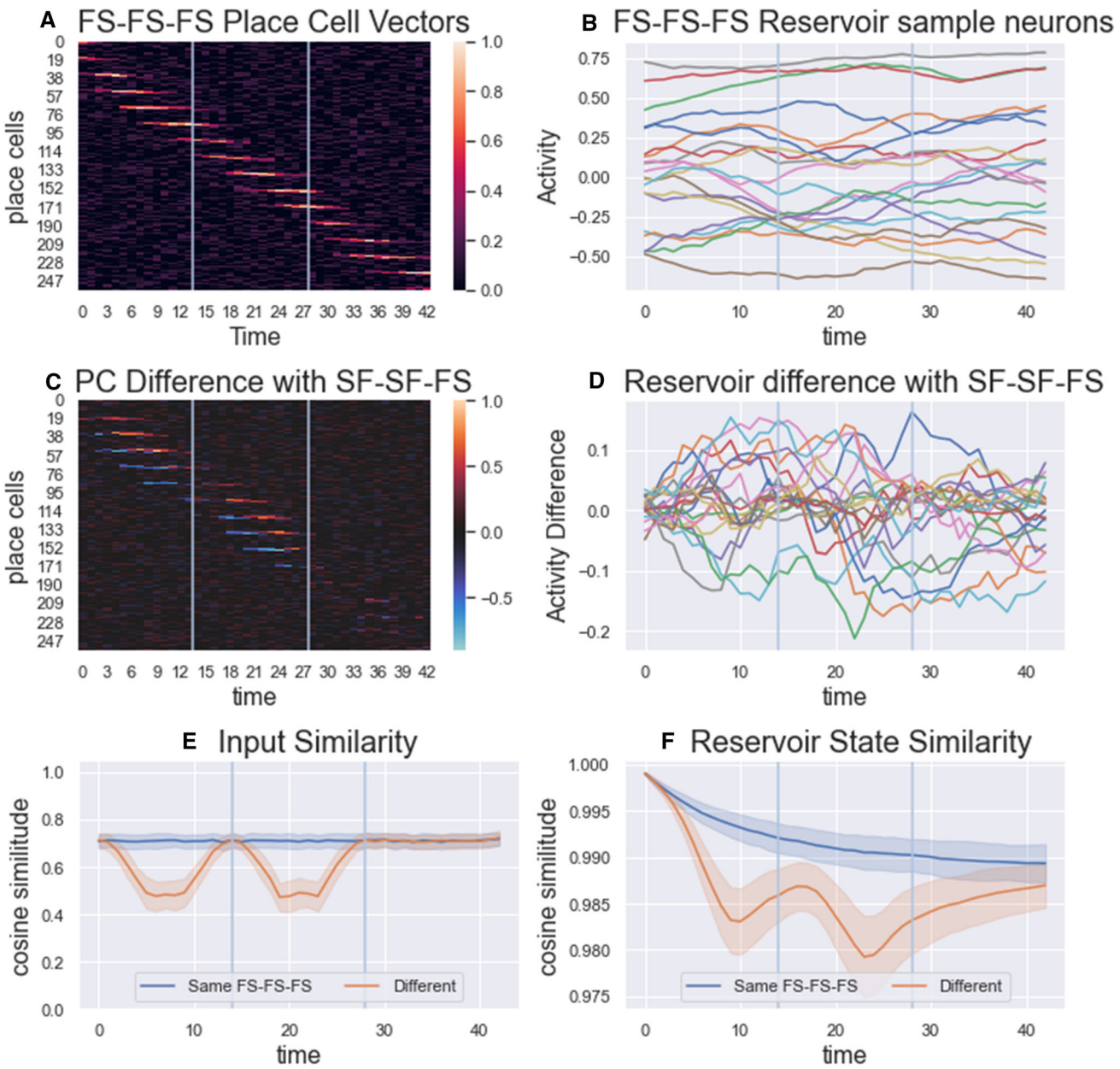

Fig. 8 Experiment 4 reservoir results using 20% localization and additive noise. **A** Sample place cell activation trajectory for sequence FS-FS-FS. **B** Activity of 20 sample reservoir units in response to speed profile FS-FS-FS. **C** Difference between the place cell activation trajectory of a sample SF-SF-FS sequence and the sample FS-FS-FS shown in panel A. **D** Same as C but taking the difference between reservoir activities. **E** Cosine similarity vs. time plots comparing 120 pairs of input sequences (i.e., the vectors of PC activities). The blue plot compares sequences of the same type (SF-SF-FS), while the red plot compares SF-SF-FS vs. FS-FS-FS sequence pairs. Dark lines indicate the mean, while shaded areas indicate the standard deviation. **F** Same information as E but calculates the similarity between reservoir states instead of input states. The light blue vertical lines on each plot indicate the three segments of each sequence. Note that similarity is initially high because reservoir pairs start in the same initial state

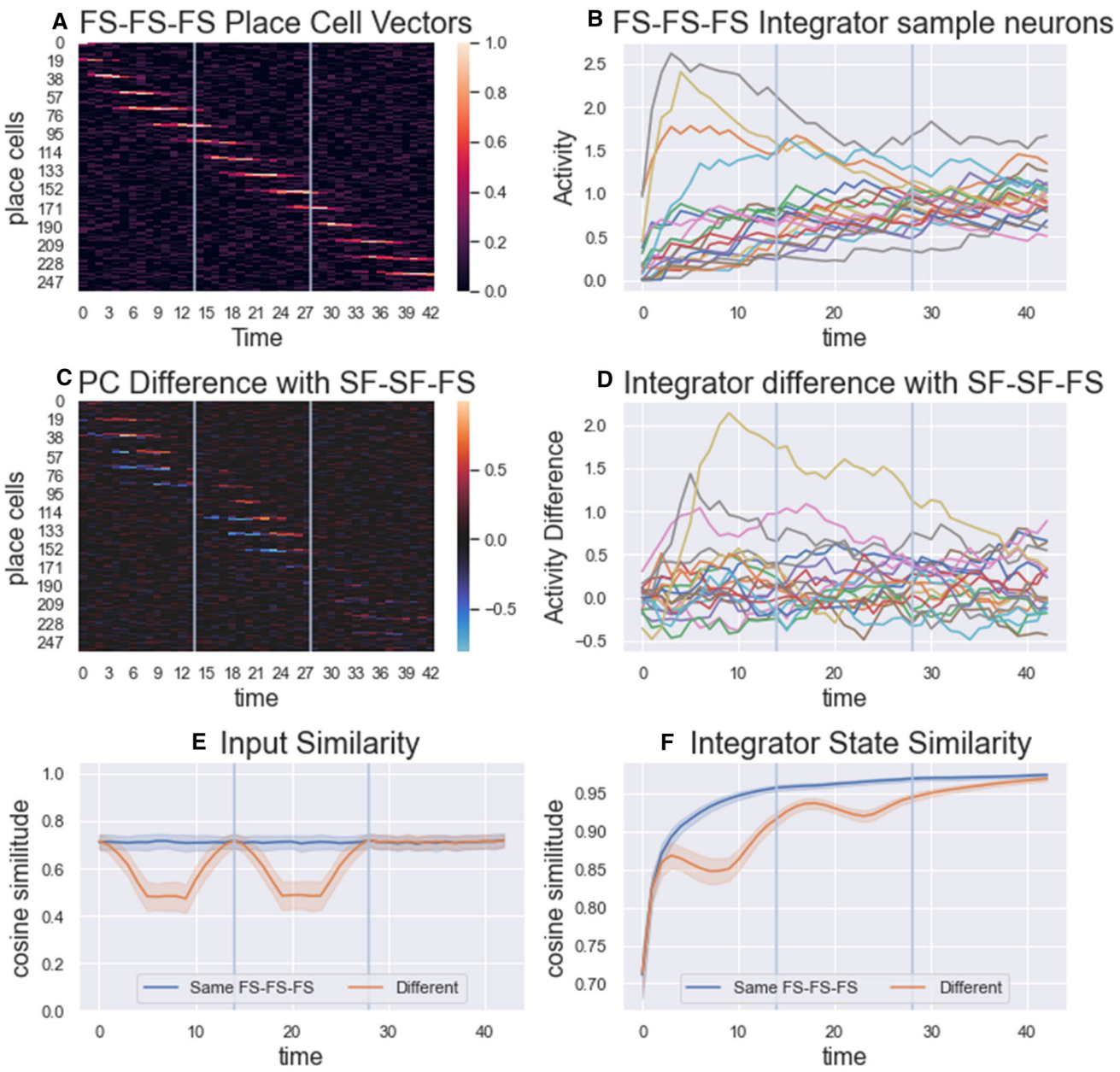

Fig. 9 Experiment 4 integrator results using 20% localization and additive noise. **A** Sample place cell activation trajectory for sequence FSS. **B** Activity of 20 sample integrator units in response to speed profile FS-FS-FS. **C** Difference between the place cell activation trajectory of a sample SF-SF-FS sequence and the sample FS-FS-FS shown in panel A. **D** Same as C but taking the difference between integrator activities. **E** Cosine similarity vs. time plots comparing 120 pairs of input sequences (i.e., the vectors of PC activities). The blue plot compares sequences of the same type (SF-SF-FS), while the red plot compares SF-SF-FS vs. FS-FS-FS sequence pairs. Dark lines indicate the mean, while shaded areas indicate the standard deviation. **F** Same information as E but calculates the similarity between integrator states instead of input states. The light blue vertical lines on each plot indicate the three segments of each sequence. The linear integrator is initialized with the first sequence of place cells as per Eq. 3. Thus, the initial cosine similarity is the same as the cosine between the inputs as observed in E and F

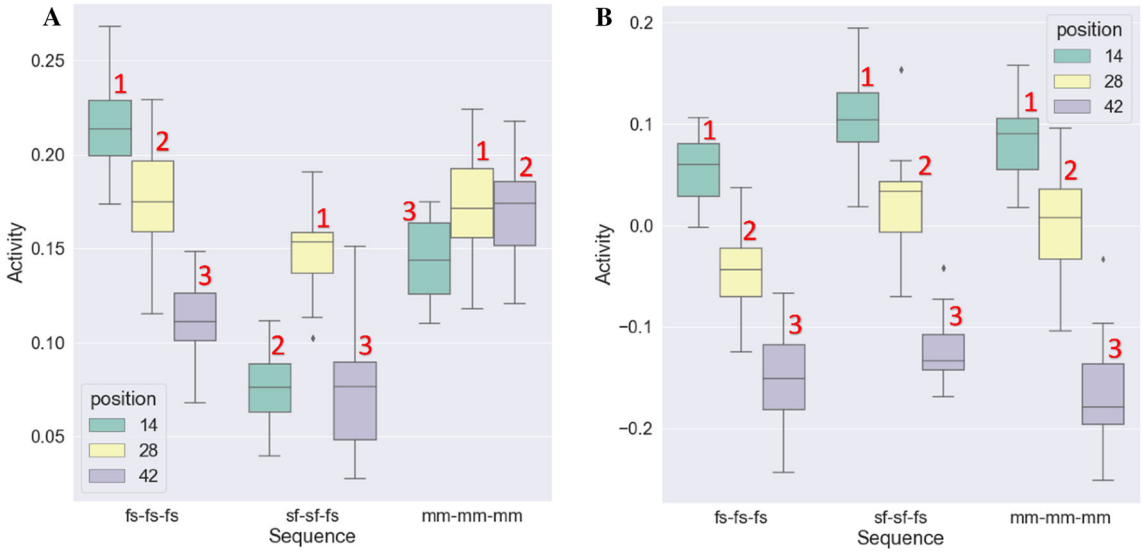

Fig. 10 Shape Change **A** Nonlinear mixed selectivity. Example of a reservoir neuron with nonlinear mixed selectivity. There is an ANOVA interaction between factors "position" (early, middle, late) and "sequence" (FS-FS-FS, SF-SF-FS, M-M-M). Note that for the three sequences, the relative activation values for the three positions change and have different shapes in each sequence (123,213,213). This shape change is the criteria for nonlinear mixed selectivity. **B** Simple mixed selectivity. Here, for the three sequences, the relative activation values for the three positions are the same for the three sequences (123,123,123)

of mixed selectivity. In Fig. 10A, we see a typical example of reservoir mixed selectivity where the relative magnitude of the responses to the position is modified as a function of the speed profile, i.e., the shape—as characterized by the relative magnitude of early vs. middle, middle vs. late, and early vs. late—is not the same for the three sequences. This shape change corresponds to the classic ANOVA interaction where the relative values of components of one factor can be reversed when considered in terms of the second factor. Figure 10B illustrates a case where the ANOVA detected mixed selectivity, where relative magnitudes were simply shifted upwards or downwards coherently across the two sections (early, mid, and late).

We systematically evaluated shape change and applied it to the PFC-reservoir and linear integrator. The method consists in assigning the relative rank for the three positions for each of the three sequences. If the three rank sequences are identical, then there is no shape change—as illustrated in Fig. 10B. If any of them are different, then there is a shape change, as illustrated in Fig. 10A. With this definition of mixed selectivity with shape change, we now observe this mixed selectivity in 81.2/256 of the reservoir neurons and 5.4 and 5 neurons in the variable and constant linear integrators, respectively (Table 4, last line).

It is particularly interesting to examine the effects of noise on these properties. We systematically tested the three models with localization noise and activation noise varying from 0 to 0.4 in 0.1 increments. A summary of these results is displayed in Fig. 11, which illustrates performance and mixed selectivity results for the three models under three noise conditions. There we see that the discrimination performance is high for low noise and degrades gracefully with full noise. We also observe that under noise conditions, the level of mixed selectivity, shape change, and the ratio of shape change to general mixed selectivity is favored in the reservoir with respect to both integrator forms.

Figures 14, 15 and 16 in appendix illustrate the number of cells in the three models under 25 different noise conditions displaying mixed selectivity, nonlinear (shape change) mixed selectivity, and the normalized number of nonlinear mixed selectivity cells (ratio between shape changing and mixed selectivity neurons). We observe in Fig. 14 that under a large range of noise configurations, the reservoir has the highest number of mixed selectivity units. This effect is emphasized for the nonlinear mixed selectivity illustrated in Fig. 15 and the normalized mixed selectivity in Fig. 16.

In the reservoir, the mix of inhibitory and excitatory recurrent connections between units produces true mixed selectivity as units interact with each other via these recurrent connections. In the Linear Integrator network, each unit is independent, and this high-dimensional mixed selectivity was less present. This generates the strong testable prediction that the rat PFC should display a high proportion of high-dimensional dynamic shape change mixed selectivity. Further rodent experiments should be conducted to test this hypothesis.

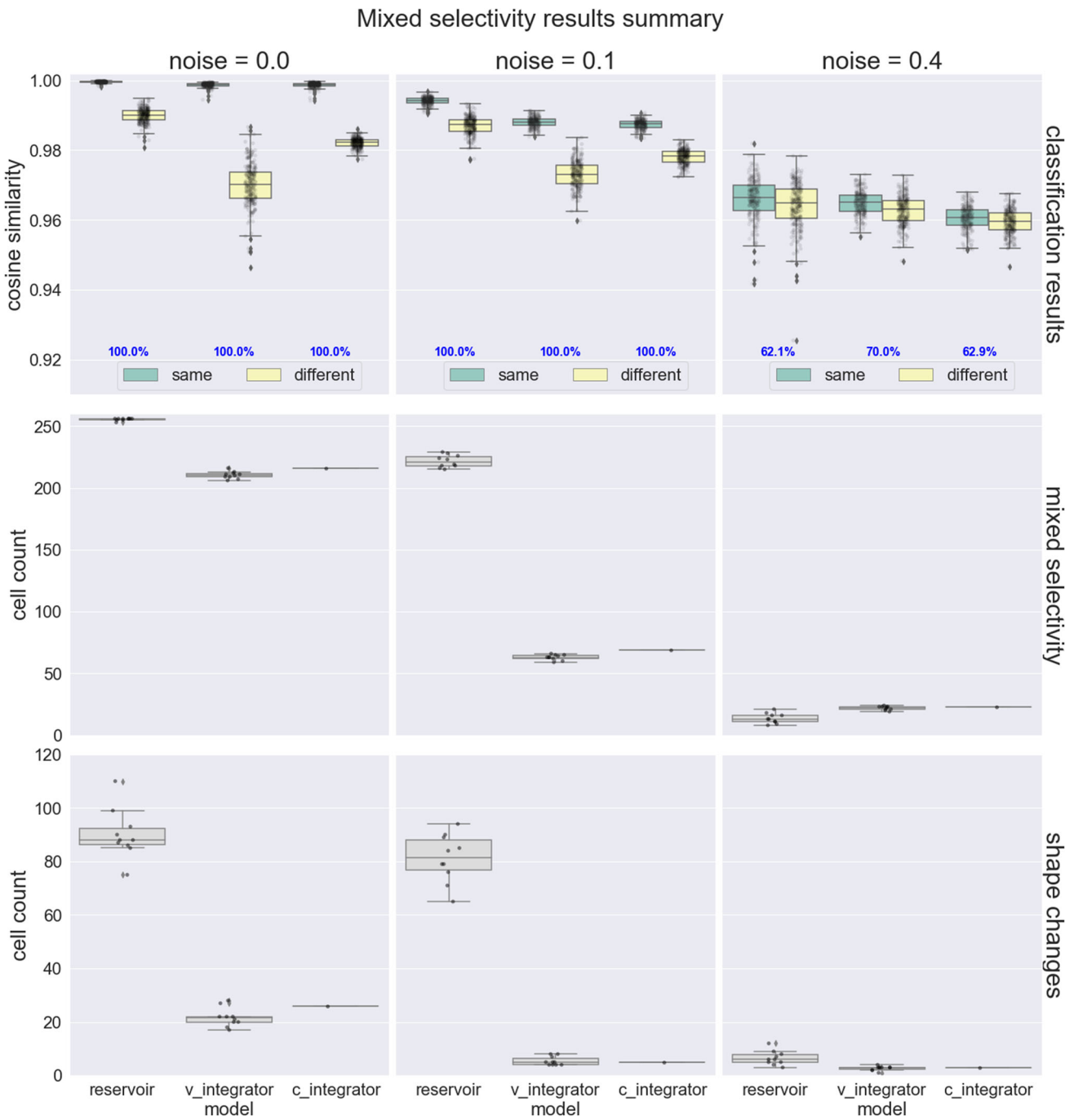

Fig. 11 Experiment 4 result summary. The image summarizes the results of the mixed selectivity experiment for the 3 models (x-axis) and the 3 different noise levels indicated by the column using the same level of additive and localization noise. The first row shows the cosine similarity distributions of the classification task using sequences FS-FS-FS and SF-SF-FS. The numbers in blue indicate the accuracies achieved by the nearest neighbor classifiers for the respective models. The second and third rows show the number of mixed selectivity and shape changing cells, and the last row shows the percentage of shape changing cells with respect to the number of mixed selectivity cells

5 General discussion

The ability to control rat navigation speed in megaspace enclosures offers a new class of experimental possibilities (Harland et al 2021). One of the most interesting is the ability to induce the rat to follow the same spatial trajectory but with different speed profiles, thus allowing for the investigation of how speed history, and thus time and its interaction with space, is represented in the nervous system. This provides a robust framework for studying the neurodynamics of the frontal cortex in tasks where space and time interact. This is interesting because such experiments would directly allow the testing of hypotheses about the possible reservoir computing properties of cortical dynamics and the coding of time and behavior in the cortex. Here we presented a set of experimental results that begin to specify and validate these hypotheses. We should note that, while the model presented here is based exclusively on HIPP place cells and PFC, there have been studies of speed modulated place cells (Góis & Tort 2018; Iwase et al 2020; McClain et al 2019), among other approaches not yet explored in this work.

In experiment 1, we demonstrated for the first time that rats in a large open space could be trained to discriminate between two velocity profiles on the same path. This exploits a new behavioral paradigm in which rats are trained to follow a small (rat-sized) robot, allowing the experimental control of both spatial and temporal (i.e., speed) features of spatial trajectories. We know that place cell coding in this robot-following condition is equivalent to that in the freely navigating animal, so this paradigm allows the exploration of spatial coding with a new level of control over the displacement of the animal (Harland et al 2021). One limitation of this experiment is that the rats could have used final speed as a decision criterion. Future experiments should use trajectories that rely on discrimination based on a past speed difference, as in those used in experiments 2–4.

Given this confirmation that the animals can indeed use their own speed profile to make a future decision, we performed simulations in which we demonstrated how a reservoir model of PFC could acquire speed profile information by integrating data from the place cell population vector. This process benefits from the experience from the distant past and the fading memory embodied by the recurrent connections. We considered a case where the reservoir experiences two speed profiles, moving with different speeds along the same straight-line trajectory. The two resulting trajectories had the same duration, started at the same speed, and ended at the same speed. However, because of the fading memory of inputs resulting from the flow of information through the recurrent connections, the internal states of the reservoir after each of these two respective trajectories were systematically different. The model (or animal) can exploit this systematic coding difference between the two trajectories to learn that one should be associated with a left turn and the other with a right turn.

This corresponds to a form of complex sequence learning, in that the successor of a given element cannot be predicted purely by that element but requires access to elements farther in the past. We have previously demonstrated the ability of such reservoir models to learn complex spatial sequences where the time dimension was uniform (Dominey 1995; Dominey et al 1995). We then explored how the model could explain human behavior in sequence learning tasks in which the same spatial sequence could be learned and tested with different temporal structures (Dominey 1998a, b). Here for the first time, we demonstrate this sensitivity in the context of distributed place-cell coding of inputs, with sequences that have identical spatial trajectories, with only the temporal component modified.

In experiment 3, we tested the PFC-reservoir in a real robotic context, where the speed profiles were generated by our own robots navigating in a large open space. This produced spatio-temporal trajectories of movement, illustrated in Fig. 5, in which the distinction between speeds in the different segments was much more subtle. In Fig. 6, we can visualize this effect in the display of the place cell vector activation trajectories for sample runs of the speed profiles FSS and SFS. The cosine similarity of the two place cell vector trajectories in panel E clearly reveals the difference between the FSS and SFS trajectories at their outsets and then the similarity at the common end with slow (S) speed. Interestingly, the cosine similarity of the two PFC-reservoir state trajectories in panel F reveals that the reservoir picks up on this difference and maintains a trace of it beyond the end of the shared final segment. That is, the reservoir can maintain the past context in its current activity at the time the decision must be made. We should note that we measured the ability of the reservoir to distinguish between different sequences by using a measure of cosine similarity for reservoir states that resulted from exposure to the same or different sequences. This is similar to (Bianchi et al 2020), where the reservoir states were used as input to a vectorial data classification algorithm. We could have equivalently trained a set of readout neurons to produce the corresponding responses.

Based on this demonstration of the PFC-reservoir's capability to maintain information that can allow future decisions about past experience, in experiment 4, we set out to determine whether this encoding would be associated with the signature mixed selectivity that is the underpinning of certain aspects of cortical cognitive function (Enel et al 2016; Ramirez-Cardenas & Viswanathan 2016; Rigotti et al 2013). In order to compare the reservoir with a spatio-temporal integration model that does not rely on between-neuron recurrent connections, we used a linear integrator model. We analyzed the neurons in the PFC-reservoir using the same methods we

previously used in analyzing primate cingulate cortex activity, and reservoir activity, in a cognitive task that manipulated an explore-exploit tradeoff (Enel et al 2016). We thus analyzed the neural activity of these neurons in the three spatial segments of the navigation trajectories using the three speed profiles in 2-way ANOVAs, with position and speed profile as factors. A large portion of neurons displayed an effect for position (99% under 0.1 noise). We interpret this as a consequence of the coding of the input in terms of activations of place cells that indeed code position. Over three-quarters of the neurons (85% under 0.1 noise) displayed a significant effect for speed profile. Importantly, over three-quarters (86% under 0.1 noise) of the neurons also displayed the position x speed profile interaction that we further used to characterize mixed selectivity.

When we compared the PFC-reservoir model with a linear integrator, an alternative model that is well adapted to integrate behavior over time, we observed that it was able to perform the speed profile discrimination task and surprisingly also displayed a moderate degree of position x speed profile interaction. Further investigation revealed that the interaction effect in the LI was due to shifts in the within-trial responses that maintained the relative magnitude of position-related responses, as illustrated in Fig. 10. In Fig. 10B we see that while the relative preference of the unit for the three positions in the 3 speed profiles is the same, the amplitudes are sufficiently different to produce the statistical interaction. In contrast, with the reservoir, the relative preference of a neuron for a given position could be completely different for each of the three sequences. In Fig. 10A we see that this reservoir unit reverses its position preference depending on the speed-profile. In the context of this dynamic response shape changing, the reservoir displayed greater mixed selectivity. The mixed selectivity effects were also significantly impacted by the introduction of noise in the place cell representations. Under these more realistic conditions (i.e., with noise and variability in the neural activity), the reservoir displayed a marked increase in the presence of mixed selectivity with respect to the linear integrators (see appendix). The mixed selectivity that we observe in the reservoir model is due to the presence of recurrent connections that allow the functional mixing of input signals and the evolving internal state.

We believe that the model features that are required to pass this test are the existence of recurrent connections between different reservoir neurons. This produces a mixing of response properties that is dependent on prior inputs. This is a natural property of recurrent networks such as reservoirs, due to the recurrent connections. In contrast, linear integrators with units that receive inputs from only a single input vector unit will not display such interactions.

Here, we focused on tests that traversed a given path in the same amount of time but using two different speed profiles, maintaining an overall same duration. These constraints were necessary to ensure that effects were due only to the speed profiles. Mixed selectivity for position and prior history could likewise be examined. The linear integrator units will reflect how recently their preferred location has been visited, while reservoir units will reflect a higher dimensional signal that is influenced by all locations that have been previously visited, which should be reflected in a sequence x position mixed selectivity with shape change.

Importantly, the reservoir does not adapt its internal dynamics to the task, thus allowing the whole and complete range of dynamic flexibility in the recurrent state representations. In future research, it will be of interest to determine whether the modification of the recurrent connections in related recurrent networks (Martinet et al 2011; Rougier et al 2005) will influence the mixed selectivity profile. Previous studies demonstrating mixed selectivity in reservoirs use factors such as object identity and task type, as in Rigotti et al (2013). In the current study, one of the factors is the temporal structure. To the best of our knowledge, no previous study has investigated mixed selectivity with temporal structure as one of the factors.

This provides an exciting new framework for studying space and time coding in the cortex in a novel megaspace navigation paradigm in which speed and direction of movement can be effectively manipulated, and that offers a substantial potential for further understanding the underlying neurophysiology and influence of speed on spatial navigation (Harland et al 2021).

Acknowledgements PFD received funding from the French Région Bourgogne Franche Comté, Grant No. ANER RobotSelf 2019-Y-10650. JMF and AW received funding from NSF-IIS Robust Intelligence Grants No. #1703340 & #1703225.

Declarations

Conflict of interest The authors declare that they have no conflict of interest.

Appendix

Details on effects of noise (localization error, additive noise) on sequence classification accuracy and cosine similarity, and mixed selectivity.

See Figs. 12, 13, 14, 15, 16.

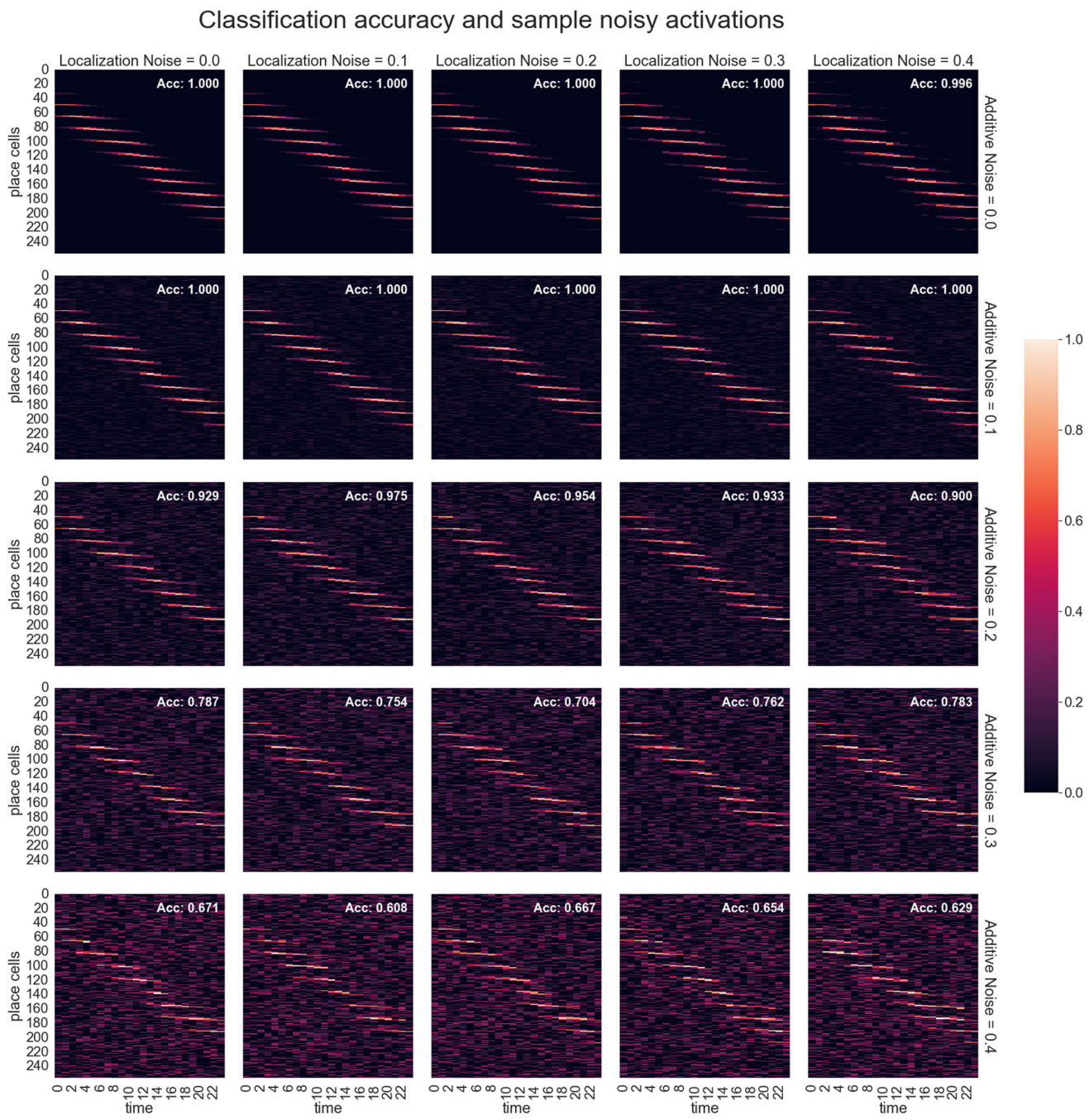

Fig. 12 Experiment 3. Noisy place cell activity. The figure illustrates a table of heat maps representing the activity of all place fields along the same path for different noise combinations. The number on the top right corner of each heatmap indicates the accuracy obtained by the reservoir in the robot classification task for each noise level

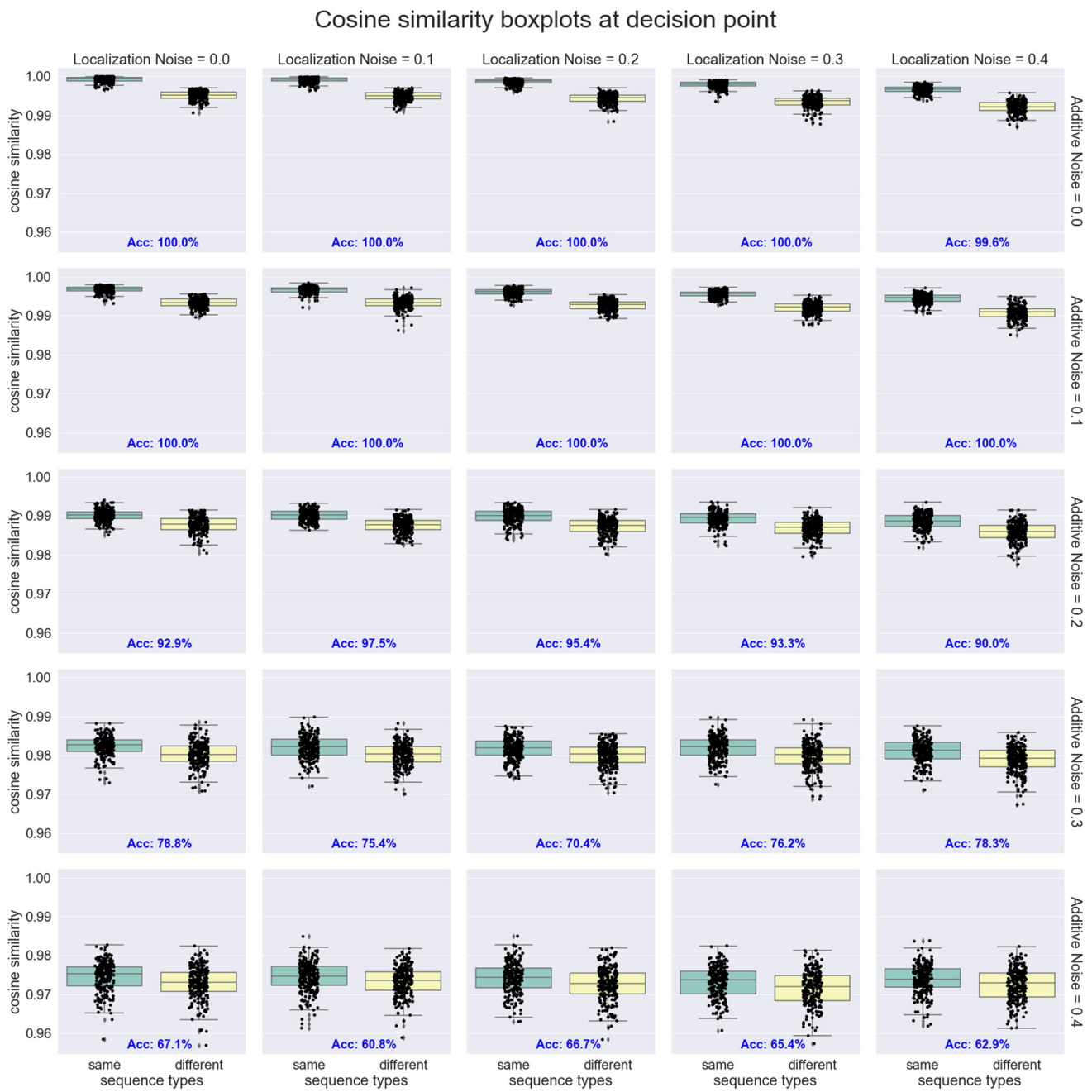

Fig. 13 Experiment 3. Noisy cosine similarities. The figure shows a table of boxplots for different noise levels illustrating the cosine similarities between reservoir states of the same and different sequence types (FSS and SFS) at the decision point. Each boxplot is composed of 240 data samples. The number in blue shown at the bottom of each plot indicates the classification accuracy obtained at each noise level. As observed, the higher the noise, the closer the distance between groups, and thus, the more complex the classifications task

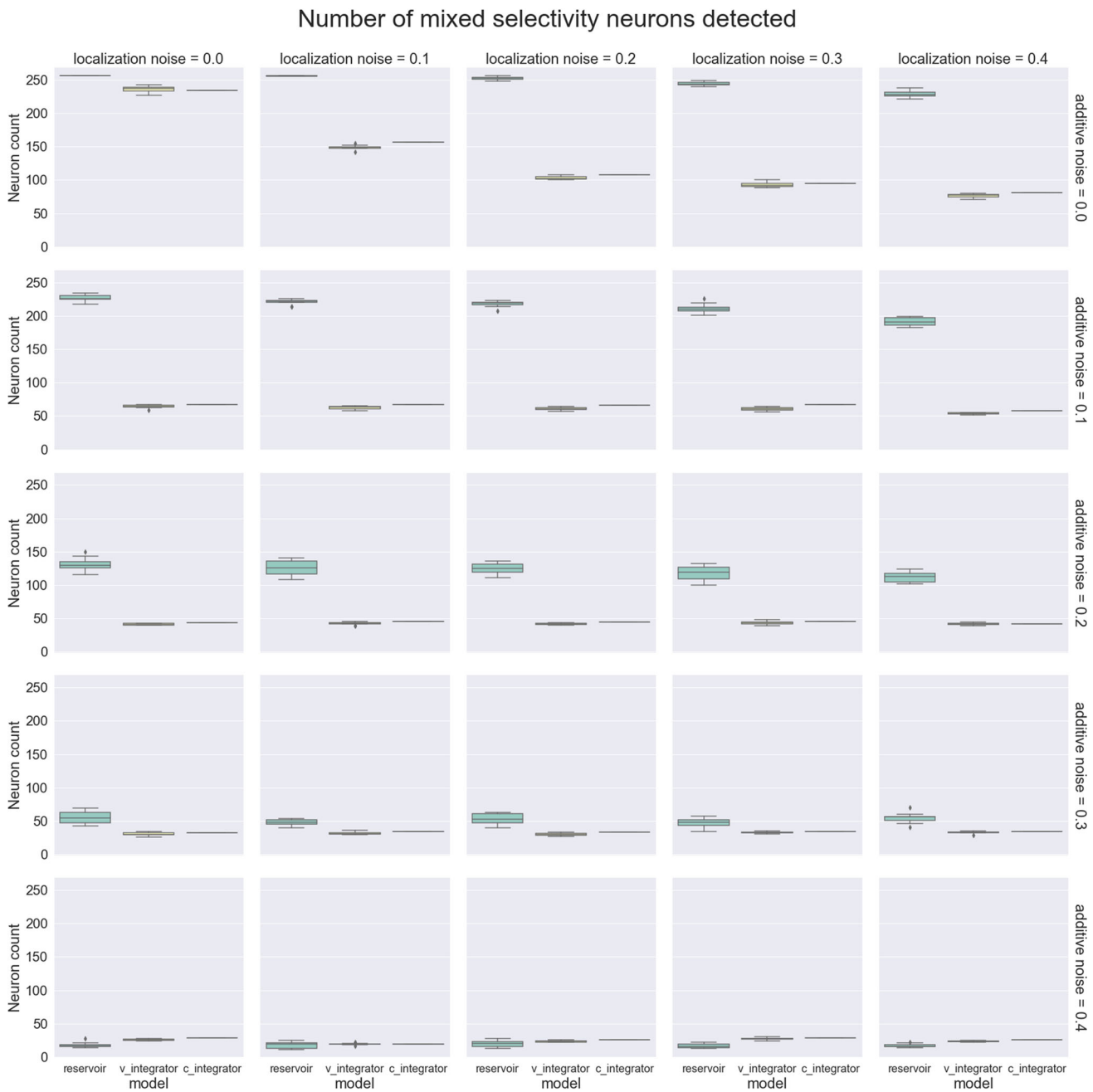

Fig. 14 Experiment 4. Number of mixed selectivity neurons. The figure illustrates a table of boxplots indicating the number of mixed selectivity neurons for the 10 reservoir models, the 10 linear integrators with variable leak rates, and the 1 linear integrator with constant leak rates. Rows and columns show results for different noise levels

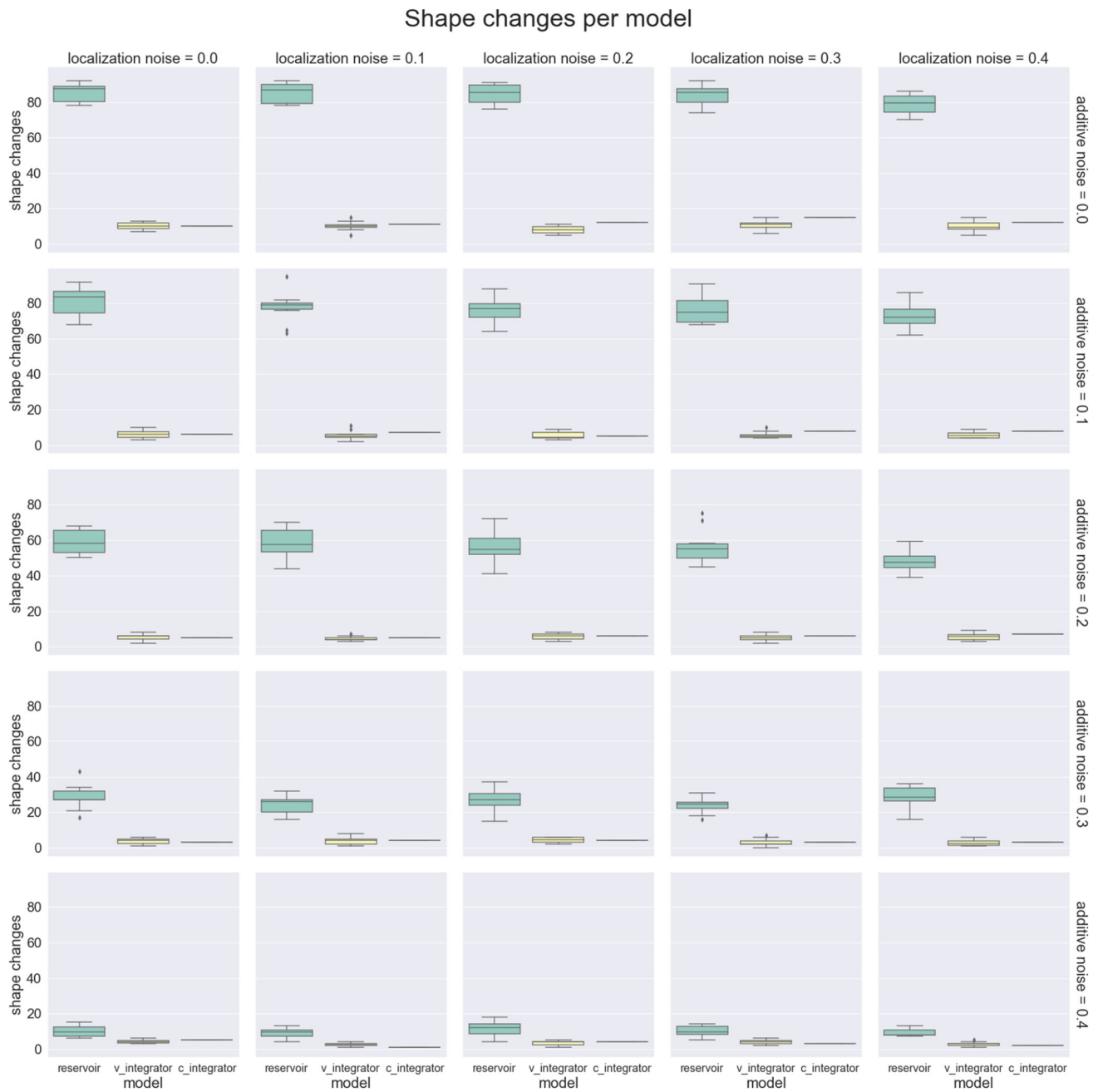

Fig. 15 Experiment 4. Number of shape changing neurons. The figure illustrates a table of boxplots indicating the number of shape changing neurons for the 10 reservoir models, the 10 linear integrators with variable leak rates, and the 1 linear integrator with constant leak rates. Rows and columns show results for different noise levels

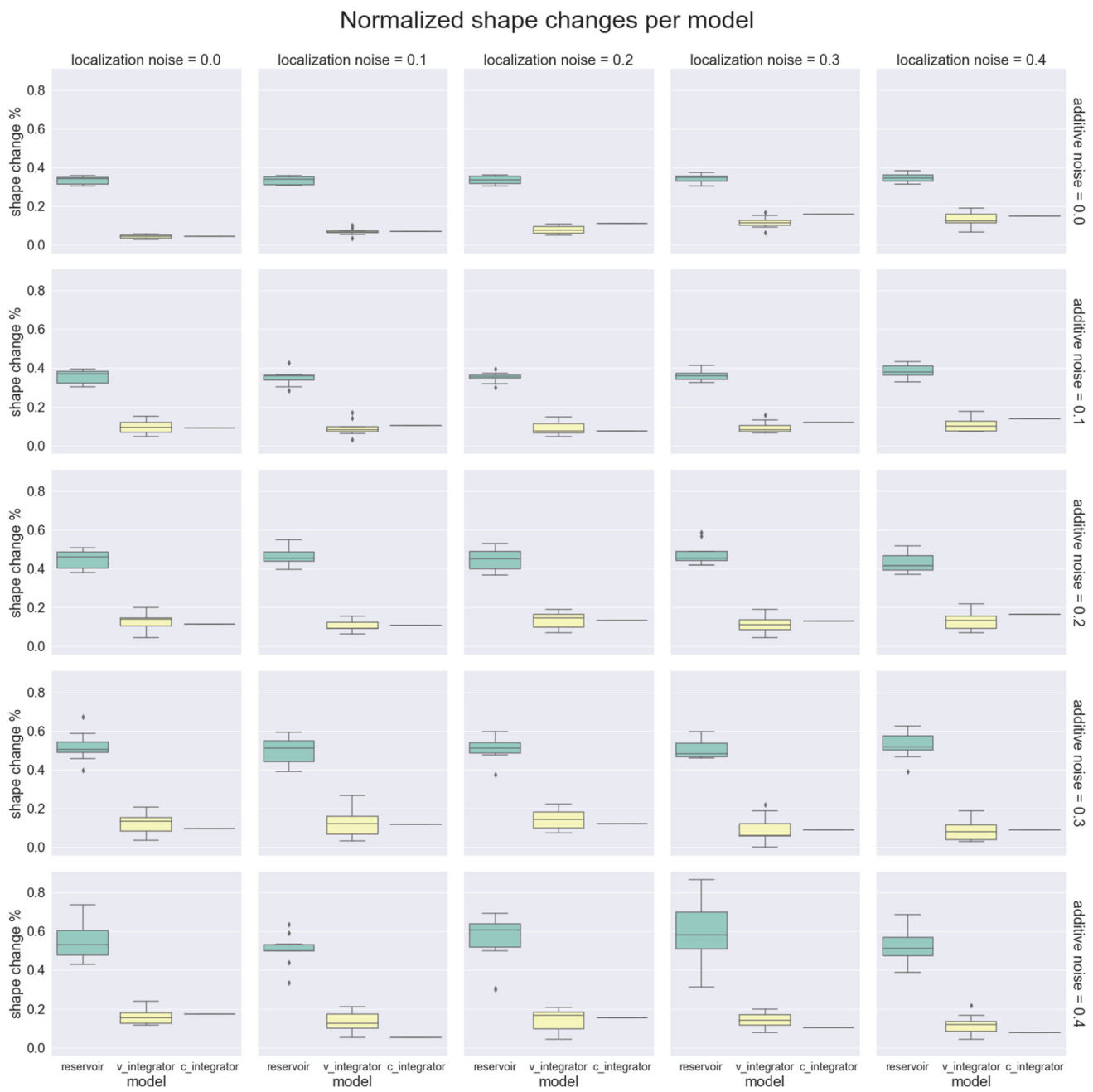

Fig. 16 Experiment 4. Normalized number of shape changing neurons. The figure illustrates a table of boxplots indicating the ratio between shape changing neurons and mixed selectivity neurons for the 10 reservoir models, the 10 linear integrators with variable leak rates, and the 1 linear integrator with constant leak rates. Rows and columns show results for different noise levels

References

Aghajan ZMAL, Moore JJ, Cushman JD, Vuong C, Mehta MR (2015) Impaired spatial selectivity and intact phase precession in two-dimensional virtual reality. Nat Neurosci 18:121–128

Arleo A, Gerstner W (2000) Spatial cognition and neuro-mimetic navigation: a model of hippocampal place cell activity. Biol Cybern 83:287–299

Barrera A, Weitzenfeld A (2008) Biologically-inspired robot spatial cognition based on rat neurophysiological studies. J Auton Robot 25:147–169

Barrera A, Caceres A, Weitzenfeld A, Ramirez-Amaya V (2011) Comparative experimental studies on spatial memory and learning in rats and robots. J Intell Robot Sys 63:361–397

Barrera A, Tejera G, Llofriu M, Weitzenfeld A (2015) Learning spatial localization: from rat studies to computational models of the hippocampus. J Spat Cognit Comput 15:27–59

Barrera A, Weitzenfeld A, Caceres A, Ramirez-Amaya V (2010) *Spatial memory and learning: towards a set of metrics to evaluate task performance in rats and robots.* In: Presented at IEEE-RAS International conference on robotics and automation, Anchorage, Alaska

Bianchi FM, Scardapane S, Løkse S, Jenssen R (2020) Reservoir computing approaches for representation and classification of multivariate time series. IEEE Trans Neur Netw Learn Sys 32:2169–2179

Bonasia KBJ, Moscovitch M (2016) Memory and navigation: compression of space varies with route length and turns. Hippocampus 26:9–12

Buonomano DV, Laje R (2010) Population clocks: motor timing with neural dynamics. Trends in cognitive sciences. Elsevier, Armsterdam, pp 71–85

Buonomano DV, Merzenich MM (1995) Temporal information transformed into a spatial code by a neural network with realistic properties. Science 267:1028–1030

Buzsaki G, Llinas R (2017) Space and time in the brain. Science 358:482–485

Caluwaerts KSM, N'Guyen S, Grand C, Dollé L, Favre-Felix A, Girard B, Khamassi M (2012) A biologically inspired meta-control navigation system for the Psikharpax rat robot. Bioinsp Biomim. https://doi.org/10.1088/1748-3182/7/2/025009

Cazin N, Llofriu M, Scleidorovich PM, Pelc T, Harland B et al (2019) Reservoir computing model of prefrontal cortex creates novel combinations of previous navigation sequences from hippocampal place-cell replay with spatial reward propagation. PLoS Computat Biol 15(7):e1006624

Cazin N, Scleidorovich, P., Weitzenfeld, A., Dominey P (2020) Real-time sensory-motor integration of hippocampal place cell replay and prefrontal sequence learning in simulated and physical rat robots for novel path optimization. Biol Cybern, Special Issue on 'Complex Spatial Navigation in Animals, Computational Models and Neuro-inspired Robots', Guest eds P. Dominey, J.M. Fellous, and A. Weitzenfeld

Chiba AAKR, Reynolds AM (1994) Memory for spatial location as a function of temporal lag in rats: role of hippocampus and medial prefrontal cortex. Behav Neural Biol 61:123–131

Chien H-YS, Honey CJ (2020) Constructing and forgetting temporal context in the human cerebral cortex. Neuron 106(675–86):e11

Dolleman-van der Weel MJGA, Ito HT, Shapiro ML, Witter MP, Vertes RP, Allen TA (2019) The nucleus reuniens of the thalamus sits at the nexus of a hippocampus and medial prefrontal cortex circuit enabling memory and behavior. Learn Mem 26:191–205

Dominey PF (1995) Complex sensory-motor sequence learning based on recurrent state representation and reinforcement learning. Biol Cybern 73:265–274

Dominey PF (1998) Influences of temporal organization on sequence learning and transfer: comments on Stadler (1995) and Curran and Keele (1993). J Exper Psychol Learn Mem Cognitio 24(1):234–248

Dominey PF (1998b) A shared system for learning serial and temporal structure of sensori-motor sequences? Evidence from simulation and human experiments. Brain Res Cogn 6:163–172

Dominey PF (2021) Narrative event segmentation in the cortical reservoir. PLoS Comput Biol 17(10):e1008993. https://doi.org/10.1371/journal.pcbi.1008993.PMID:34618804;PMCID:PMC8525778

Dominey PF, Ramus F (2000) Neural network processing of natural language: I. sensitivity to serial, temporal and abstract structure of language in the infant. Lang Cognit Process 15:87–127

Dominey PF, Arbib MA, Joseph JP (1995) A model of corticostriatal plasticity for learning oculomotor associations and sequences. J Cogn Neurosci 7:25

Eichenbaum H (2014) Time cells in the hippocampus: a new dimension for mapping memories. Nat Rev Neurosci 15:732–744

Enel P, Procyk E, Quilodran R, Dominey PF (2016) Reservoir computing properties of neural dynamics in prefrontal cortex. PLoS Comput Biol 12:e1004967

Ercsey-Ravasz M, Markov NT, Lamy C, Van Essen DC, Knoblauch K et al (2013) A predictive network model of cerebral cortical connectivity based on a distance rule. Neuron 80:184–197

Filliat D, Meyer, JA (2002) From animals to animats: 7 proceedings of the seventh international conference on simulation of adaptive behavior.pp. 131–40. MIT Press

Furtunato A, Lobão-Soares B, Tort A, Belchior H (2020) Specific increase of hippocampal delta oscillations across consecutive treadmill runs. Front Behav Neurosci. https://doi.org/10.3389/fnbeh.2020.00101

Fusi S, Miller EK, Rigotti M (2016) Why neurons mix: high dimensionality for higher cognition. Curr Opin Neurobiol 37:66–74

Geisler CRD, Zugaro M, Sirota A, Buzsaki G (2007) Hippocampal place cell assemblies are speed-controlled oscillators. Natl Acad Sci 104:8149–8154

Gianelli SHB, Fellous JM (2018) A new rat-compatible robotic framework for spatial navigation behavioral experiments. J Neurosci Methods 294:40–50

Góis ZHTD, Tort ABL (2018) Characterizing speed cells in the rat hippocampus. Cell Rep 25:1872–1884

Goldman-Rakic PS (1987) Circuitry of primate prefrontal cortex and regulation of behavior by representational memory. Handbk Neurophys 5:40

Harland B, Contreras M, Souder M, Fellous J-M (2021) Dorsal CA1 hippocampal place cells form a multi-scale representation of megaspace. Curr Biol 31(2178–90):e6

Hinaut X, Dominey PF (2013) Real-time parallel processing of grammatical structure in the fronto-striatal system: a recurrent network simulation study using reservoir computing. PloS one 8(2):e52946

Honma MKT, Futamura A, Shiromaru A, Kawamura M (2016) Dysfunctional counting of mental time in Parkinson's disease. Sci Rep. https://doi.org/10.1038/srep25421

Huk AC, Shadlen MN (2005) Neural activity in macaque parietal cortex reflects temporal integration of visual motion signals during perceptual decision making. J Neurosci 25:10420–10436

Iwase M, Kitanishi T, Mizuseki K (2020) Cell type, sub-region, and layer-specific speed representation in the hippocampal-entorhinal circuit. Sci Rep 10(1):1–23

Jaeger H, Maass W, Principe J (2007) Special issue on echo state networks and liquid state machines. Neural Netw 20:287–289

Jan T, Adrien F, Yulia S, Gregor S (2019) Autonomous sequence generation for a neural dynamic robot: scene perception, serial order and object-oriented movement. Front Neurorob 13:95

Kraus B, Robinson R, White J, Eichenbaum H, Hasselmo M (2013) Hippocampal "time cells": time versus path integration. Neuron 78:1090–1101

Laje R, Buonomano DV (2013) Robust timing and motor patterns by taming chaos in recurrent neural networks. Nat Neurosci 16:925–933

Lashley KS (1951) The problem of serial order in behavior. Bobbs-Merrill, Oxford

Llofriu M, Tejera G, Contreras M, Pelc T, Fellous JM, Weitzenfeld A (2015) Multi-scale space representation and learning in goal-oriented robot navigation. J Neur Netw 72:62–74

Llofriu M, Scleidorovich P, Tejera G, Contreras M, Pelc T, Fellous JM, Weitzenfeld A (2019) *A computational model for a multi-goal spatial navigation task inspired in rodent studies.* Presented at IJCNN 2019, Budapest, Hungary

Lukosevicius M, Jaeger H (2009) Reservoir computing approaches to recurrent neural network training. Comp Sci Rev. https://doi.org/10.1016/j.cosrev.2009.03.005

Maass W, Natschläger T, Markram H (2002) Real-time computing without stable states: a new framework for neural computation based on perturbations. Neural Comput 14:2531–2560

Martinet L-E, Sheynikhovich D, Benchenane K, Arleo A (2011) Spatial learning and action planning in a prefrontal cortical network model. PLoS Comput Biol 7:e1002045

Mauk MD, Buonomano DV (2004) The neural basis of temporal processing. Annu Rev Neurosci 27:307–340

McClain K, Tingley D, Heeger DJ, Buzsaki G. (2019) Position-theta-phase model of hippocampal place cell activity applied to quantification of running speed modulation of firing rate. Proceedings of the national academy of sciences of the United States of America

Milford M, Wyeth G (2010) Persistent navigation and mapping using a biologically inspired SLAM system. Int J Robot Res 29:1131–1153

Pastalkova E, Itskov V, Amarasingham A, Buzsaki G (2008) Internally generated cell assembly sequences in the rat hippocampus. Science 321:1322–1327

Paton JJ, Buonomano DV (2018) The neural basis of timing: distributed mechanisms for diverse functions. Neuron 98:687–705

Ramirez-Cardenas A, Viswanathan P (2016) The role of prefrontal mixed selectivity in cognitive control. J Neurosci 36:9013–9015

Rigotti M, Barak O, Warden MR, Wang XJ, Daw ND et al (2013) The importance of mixed selectivity in complex cognitive tasks. Nature 497:585–590

Rougier NP, Noelle DC, Braver TS, Cohen JD, O'Reilly RC (2005) Prefrontal cortex and flexible cognitive control: rules without symbols. Proc Natl Acad Sci 102:7338–7343

Salman H, Singhal P, Shankar T, Yin P, Salman A, et al. (2018) Learning to sequence robot behaviors for visual navigation. *arXiv*

Schmidt B, Duin AA, Redish AD (2019) Disrupting the medial prefrontal cortex alters hippocampal sequences during deliberative decision making. J Neurophysiol 121:1981–2000

Scleidorovich P, Llofriu, Fellous, JM, Weitzenfeld A (2020) a computational model for spatial cognition combining dorsal and ventral hippocampal place field maps: multi-scale navigation. Biol Cybern, Special issue on 'complex spatial navigation in animals, computational models and neuro-inspired robots', Guest Editors Dominey P, Fellous JM, Weitzenfeld A

Tejera G, Llofriu M, Barrera A, Weitzenfeld A (2018) Bio-inspired robotics: a spatial cognition model integrating place cells, grid cells and head direction cells. J Intell Robot Sys 91:85–99

Tejera G, Barrera, A., Llofriu, M., and Weitzenfeld A (2013) Solving uncertainty during robot navigation by integrating grid cell and place cell firing based on rat spatial cognition studies. Presented at ICAR 2013, Montevideo, Uruguay

Tejera G, Llofriu, M., Barrera, A., and Weitzenfeld A (2015) A spatial cognition model integrating grid cells and place cells. Presented at IJCNN 2015, Killarney, Ireland

Thiede LA, Zimmermann RS. (2017) Easyesn: a library for recurrent neural networks using echo state networks